Universidad del País Vasco Euskal Herriko Unibertsitatea
BILBOKO INGENIARITZA ESKOLA
ESCUELA DE INGENIERÍA DE BILBAO

MÁSTER UNIVERSITARIO EN INGENIERÍA INDUSTRIAL

TRABAJO FIN DE MÁSTER

UNDERSTANDING FLOWS OVER A CHANNEL FLOOR WITH CROSS-SECTIONAL JOINTS

Estudiante *Poza Sánchez, Patricia*
Director/Directora *Pinto Cámara, Charles Richard*
Departamento
Curso académico *2021-2022*

Preface

First of all, I wish to thank James Yang for giving me the opportunity to do this thesis and providing me any help I have needed during the project. Also, I would like to show my deepest gratitude to Mr. Shicheng Li at KTH Royal Institute of Technology for guiding me through the process of learning the simulation tool and helping me with any problem a have encountered during the project.

I would also like to thank Vattenfall Research and Development laboratories for making this project reality and providing all the necessary tools for it.

Finally, thanks to my supervisor, Professor Arman Ameen at the University of Gävle (HIG) for helping me with the Fluent and guiding me in the writing of the thesis.

Abstract

One of the main elements of hydraulic plants are the spillways. The main purpose of this element is to discharge water from the basin when it reaches levels above the safety limits. Therefore, spillways are designed to withstand large water flows and high pressures. However, poor channel design can lead to high pressures at the joints of the concrete slabs that make up the channel and result in fatal landslides. Clear examples are the accidents at Oroville Dam in 2017, Dickinson Dam in 1954, and Big Sandy Dam in 1983. The objective of this project is to develop a numerical model to analyze the behavior of the flow over the spillway and to study the relationship between the flow velocity and the uplift pressures generated at the channel slab joints.

For this purpose, a lot of research have been made in the field trying to understand the water behavior over a spillway, but few have focused on the uplift pressures under the slabs due to the stagnation of the water. Some experiments made by the Bureau of Reclamation analyzed the flow over the joint for different situations. In 1976, Mr Perry L. Jonshon studied experimentally the pressures generated on the linings in an open channel, while Warren Frizell tested, in 2007, the pressures under the slabs in a close water tunnel. The aim of the current project was to develop a numerical model to predict accurately the behavior of the flow over the joints and compare it to the experimental results.

Computational Fluid Dynamics (CFD) has been used as the main tool in the numerical analysis. This software has been continuously used by many scientists during the years and many investigations have verify the accuracy of the tool to predict the fluid over a spillway. Three different joint geometries have been studied, sharp-edged, chamfer-edged and radius edged joints. All the cases have been analyzed for sealed and vented situations and compared between them.

The current project has obtained great results regarding the uplift pressures and flow behavior over the joints compared to the experimental tests. The numerical model shows a maximum of 6% of deviation related to the experimental results for sealed configurations, while the vented configurations take deviations of around 15%. This increase is expected to be due to the lack of information of the discharge flow rate, for this reason, the results related to the analysis over a slope with a free surface are considered trusty enough. The study shows similar results for different slopes configurations which explains that the gravity is not the main force of the study as it was previously expected.

Contents

Figures

Tables

1 Introduction

1.1 Background

According to Zhong and Rönnberg (2021), hydroelectricity is one of the world's largest renewable energy sources, supplying 16% of global electricity demand. This value is considerably higher than other renewable energy sources such as solar and wind power. In the case of Sweden, in 2019, the country generated 164.4 TWh from which the 58% was based on renewable energies. In the first position of renewable sources was hydroelectric power, which generated 39.3% of the country's energy, making it the most important source. In second place were nuclear and thermal energy, producing 39.1%, followed by wind energy, which accounted for 12.1% of total production. Wind energy has increased its capacity considerably in recent years since 2009 when it only produced 1.27% of the country's total capacity, and is expected to develop further in the near future, but nowadays, hydropower is still Sweden's primary source (Zhong, Bollen & Rönnberg 2021).

However, there is much debate worldwide as to whether hydropower should be considered renewable or not. Due to a number of negative effects, it can cause on the environment, such as the alteration of the natural habitat of different species, the impact on the temperature and flow of the river itself, or the possibility of a series of failures in the dam mechanism that can lead to floods or other disasters. However, this technology provides a large number of positive effects too, such us the secure water supply, the control over the level of water in the reservoir, and the possibility to provide energy with almost no emissions and low cost (Frey & Linke, 2002). In this way, it is important to keep working in this technology in order to improve the system and security of the dams.

One of the most important elements of a dam is the spillway. This component is a concrete channel whose main function is to drain the dam when it reaches critical levels or levels above the safety limits. This element is generally made up of concrete slabs connected one after the other to form a channel that can be up to 1 km long. The great heights and the capacity that these elements have to withstand on a daily basis mean that they work with water velocities that can be harmful for the structure of the spillway (Karim & Mohammed, 2020).

This study, will focus specifically in the joints between the concrete slabs that compose the spillway. These cracks are usually sealed with waterstops in order to prevent the transmission of the high pressures applying in the upper part of the slabs to the foundation. The failure of this elements would allow the water flowing through the joints and getting stagnated, generating high uplift forces under the slab (Melo, Pinheiro & Ramos, 2006). This problem has been the source of several accidents during the history and therefore, it is essential to design this component correctly and to carefully study the effect of these velocities on the concrete channel so that accidents do not occur.

One of the most widely used tools for this type of calculation is Computational Fluid Dynamics (CFD), which allows different simulations to be completed quickly and efficiently. Sometimes a physical model can also be used, but this requires a lot of space and time. In this project, a study will be carried out with the Ansys simulation software, specifically Ansys Fluent.

1.2 Spillway designs

As explained above, the spillway of a dam is the element that releases water from the reservoir when it reaches critical levels. This element is a channel of different lengths and geometries, depending on the characteristics of the dam, that works continuously with large water flows. The most common geometry is the so-called ogee spillway, which is the most basic one as it is a simple discharge chute. An example is shown in Figure 1.

Figure 1-Ogee crest spillway example

The channel of the spillway is made by concrete slabs. They can be easily distinguished in the figure as the water gets stagnated in the joints showing the width of each slab. When analyzing this element in order to study the water behavior it is important to take into consideration the roughness of the material as it can have a big effect in the water velocity and pressures (Kim & Park, 2005).

One of the main purposes of these elements is related to the energy dissipation. For this reason, different techniques have been studied during the years in order to increase the energy dissipation through the channel and lower the velocity of the flow. One of the most common used techniques are the stepped spillways (Fen, Kozlov & Rumyantsev, 2016). This elements act as roughness for the water flow and reduce the acceleration of the fluid and hence the terminal velocity. This kind of spillway can also reduce the longitude of this energy dissipation element in a large percentage due to its shape, which results in less construction time and cost (Tabbara, Chatila & Awwad, 2005).

The flow over this kind of spillways can be divided into three regimes, nappe, transition and skimming which differ in the dissipation values, obtaining lower values in the nappe flows and the highest ones in the skimming (Tabbara, Chatila & Awwad, 2005). In Figure 2 it is shown the different flow regimes.

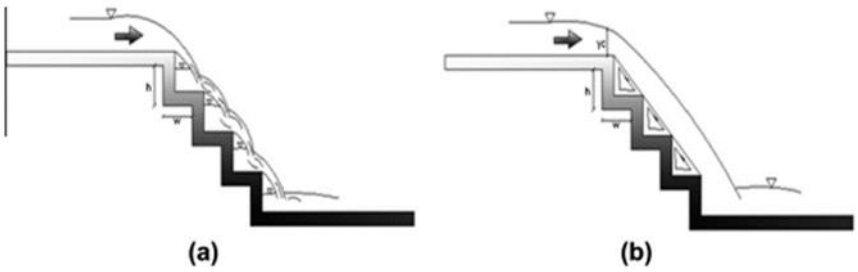

Figure 2- Flow regim through a stepped spillway: a) nappe flow and b) skimming flow (Tabbara, Chatila & Awwad, 2005)

Parsaie & Haghiabi (2019) found that an increase in the number of steps keeping the slope constant, decrease the energy dissipation. Increasing the slope with the same number of steps have a negative effect in the hydraulic efficiency of the element.

As stated before, an inappropriate design of this elements can lead to a release of the slabs which can result in a fatal disaster, it is called hydraulic jacking and will be explained more deeply in the next section as it is the main point of the study. However, other relevant consequences might also occur due to the pressure gradient in the joints, such us cavitation. It is a phenomenon that occur when the vapor pressure equals the local pressure of a liquid so that there is a phase change from liquid to vapor. It can happen due to the increase of the liquid temperature that lowers the vapor pressure in a local constant pressure, this process is called boiling. But also, it might occur due to the decrease of the local pressure keeping the temperature constant and reaching the same value as the vapor pressure at this temperature, this is called cavitation (Frizell, Rena & Matos, 2013).

When the water flow through a joint, the liquid develops a negative gradient of pressure just after the crack which can lead to really low values of pressure. These values can produce cavitation at this point of the crack that can be extremely harmful for the structure. This is more likely to occur in smooth crest than in stepped ones. Even though it is not the main purpose of the current study, further analysis is needed in order to build a proper design of a spillway (Frizell, Rena & Matos, 2013).

1.3 Hydraulic jacking

As mentioned before, one of the most dangerous problems due to the hydropower plants are the failures that might occur in the different mechanisms that can lead to fatal disasters from a failure in the dam of the reservoir to a release of the concrete that can result in fatal floodings. This project will be focused specifically in the spillway of the plant and the failure due to the uplift pressures generated below the concrete slabs of it. As stated before, the function of a spillway is to discharge the water from the reservoir when the level is above the security height. The water coming from the dam, has a large quantity of potential energy due to the height, and as it flows down the downstream spillway is transformed into kinetic energy, which increases the velocity of the fluid. When this flow stagnates against an offset in a joint, the water losses the velocity generating high pressures under the slabs, which leads to huge forces acting to lift this element, as seen in Figure 3. For example, the uplift pressure generated due to the stagnation of a fluid with a velocity of 30 m/s is 46 meter water gauge (Frizell et. al, 2019). If this force overcome the weight of the slab, the pressure that the water applies into the upper face of the slab due to its weight, and the additional structural forces regarding the lining and the anchorage, the lining may be displaced or lifted from the foundation and structural failure might occur. A lot of research has been also made in order to find correct design for the anchorage of the slab in order to avoid any kind of release (Fiorotto & Salandin, 2000). If one slab of the entire chute is displaced or even lost, it can easily lead to a successive loss of consecutive slabs which may finish in a potential large-scale disaster.

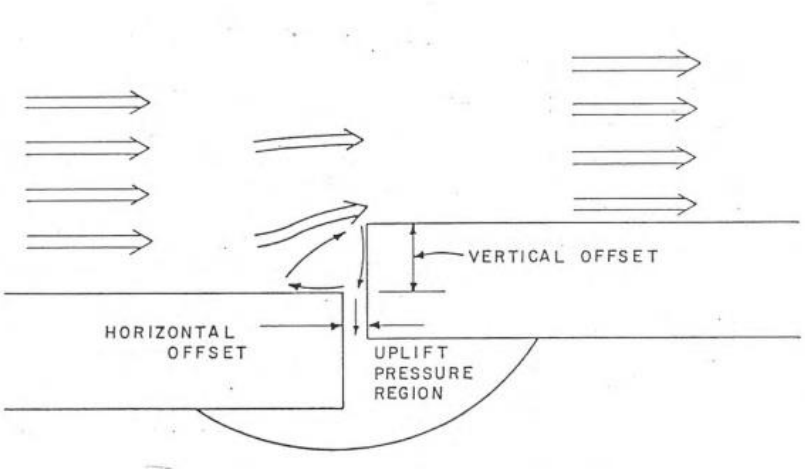

FIGURE 3-WATER BEHAVIOR THROUGH THE JOINT

1.4 Previous cases

1.4.1 Oroville dam (California)

According to Frizell (2019), one of the greatest accidents due to the uplift pressures in a spillway took place in the Oroville Dam in 2017, which was operated by California Department of Water Resources (DWR). This Dam had two discharge spillways, the first one described as the service spillway which had 8 gates that led the fluid to a concrete chute of 54.5 m wide and 914 m long, while the emergency spillway was 518 m long. The first one, had a design discharge capacity of 7.08 m^3/s, but the historical maximum flow rate discharge had been 4.53 m^3/s in 1997. The spillway had been operating for 49 years with usual flow rates above 2 m^3/s without any problem, but it was in February 2017, when the flow discharge was being increased from 1.2 to 1.49 m^3/s that the release of the concrete slab occurred. One hour later, the gates were completely closed and the damage shown in Figure 4 was revealed (Frizell et. al, 2019).

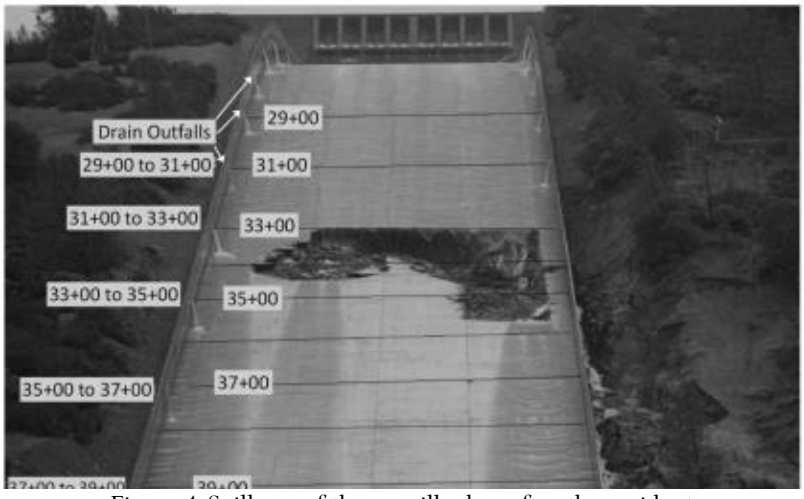

Figure 4-Spillway of the oroville dam after the accident

This accident is related to the high pressures generated in the concrete floor of the spillway due to the high fluid velocities reached during the discharge of the dams. However, it is not yet known exactly the reason why the release happened in this moment as it had previously been working with higher flows of water without any damages. There are some factors that could have affected the spillway conditions, such us the deterioration of the slabs, the expansion of the gaps under the slabs due to erosion or the reduction of the anchor capacity. Anyway, further researcher is needed in the field in order to have a good understanding about the behavior of the concrete related to the water flow rate.

1.4.2 Dickinson Dam (North Dakota)

This Dam was located on the Heart River near Dickinson and was built by the Bureau of Reclamation in the years 1949 and 1950. The service spillway was a rectangular chute of 61 m long. The spillway had been operating successfully during the first three years since it was constructed with a maximum discharge measured until the moment of 90 m^3/s in 1952.

In April of 1954 the spillway failed when it was discharging 110 m^3/s. In one day, four concrete slabs were cracked and rose above the water. The flow that entered through the cracks downside the slabs softened the foundation until they were released and floated down the spillway. After the accident, some research found that the foundations where damaged until 1.8 to 3.6 m depth.

The slabs of the chute were 380 mm thick and the had a drain mechanism composed by pipes. However, waterstops, anchor bars and foundation grouting were not built. The low temperatures under zero degrees and the inadequate insulation system lead to a failure in the drain system of the slabs. Due to the structural capacity of the slabs in these conditions, just a third of the mean velocity head would be enough to result in the observed failure. Considering a mean velocity of the flow of 6.4 m/s and a 3.2 mm of horizontal gap in the joints, just a 5 mm of vertical offset would have been enough to create the required uplift pressure for the slab release (Heplerl & Johnson, 1988)

1.4.3 Big Sandy Dam (Wyoming)

Big Sandy Dam is situated was the Big Sandy River in the north of Rock Springs in Wyoming. The spillway in this case consisted in 52 m long channel discharging into a trapezoidal chute. The construction was finished in 1952 and soon after, it started to develop different cracks in the concrete walls due to the low temperatures of the winter. This part of the chute did not have any drain system, and it was decided to make some holes in order to improve the drainage of the area.

The spillway had operated correctly several years without any accident but the discharges never exceeded the 14 m^3/s, a value that was far below the maximum capacity 208 m^3/s. During normal operation, the only outlet for the drains above a certain point was full, and water jets appeared in the holes drilled through the sabs. This meant that the water was flowing to the foundation through the joints, during the discharges. Finally, in 1983, with a discharge rate not larger than 11 m^3/s the slabs failed due to the uplift pressure (Heplerl & Johnson, 1988).

1.5 Literature review

Computational Fluid Dynamics (CFD) is a widely known software among the scientists that provides the tools to carry out accurate simulations of different fluid dynamic problems. In this case, this simulation software has been many times used for simulating the behavior of the water flow over a spillway. Also, different situations that can occur due to the flow velocity or the generated pressures in the chute have been previously studied. For this reason, there is a great interest in verifying the capability of this software in different cases in order to check the accuracy of the results obtained by comparing them with experimental tests (Fadaei-Kermani & Barani, 2014)

Recent studies have been done in this area which show the accuracy of the software in the numerical modelling of the water flow over different spillways.

Savage and Johnson (2001) compared the flow parameters of a standard ogee-crested spillway using a physical model and numerical simulations. Ten different cases were studied in the experimental tests and contrast with the numerical models obtaining good results for pressures and flow rates.

Kim and Park (2005) investigated the flow over an ogee-spillway taking into consideration the roughness and the scale effects. They found that the effect of the scale in the results are into an acceptable range of error provided that the length scale ratio is less than 200.

Dargahi (2006) studied the flow over a free-surface spillway with the CFD and predicted the water behavior and the discharges coefficients within a 1.5-2.9% of error compared to the physical model.

Zhenwei et al. (2012) studied the flow characteristics over a spillway with the VOF method, two phase model and the standard k-ε turbulence method with the fluent, and he obtained results of the pressure, the velocities and the surface elevation with an accuracy of the 6% related to the experimental tests.

All these researches where focused in the water behavior through the overall spillway obtaining results of velocity and pressure in the entire chute. However, few studies have been made focusing specifically in the high pressures that are generated in the joints of the slabs due to the flow stagnation. Two of the main studies in the field were made by the Bureau of Reclamation by Johnson in 1976, which studied the flow over the joints in open channel tests. The other one was made by Warren K. Frizell in 2007 who did the experiment in a water tunnel. In the current project, the experimental results obtained by the second study will be compared to the numerical simulations that will be carried out with the CFD, and new geometries will be studied.

1.5.1 Open channel tests (Johnson, 1976).

The aim of this study was to understand the uplift forces generated under the slabs when the flow passes through the joints. The linings can develop horizontal offsets, when the slab is displaced in the direction of the flow or vertical offsets when the displacement is perpendicular to the flow. For carrying out the experiments, a two-dimensional model of 6-inch wide and 8-feet long channel was built. In order to study the different offset configurations, the last 3-feet of the model was movable so that all the offset lengths could be measured. The slabs where 2-1/2 inches thick and under them there was a watertight pocket in order to measure the uplift pressures on it.

There were number of limitations in the model that affected the results significantly. First, the model was two-dimensional which was far from the reality and just allowed to study the water behavior in the centerline of the channel. Second, the simplicity of the model only allowed it to generate offsets normal to the plane or to the floor, but there are infinite planes where the displacements could occur in the reality. Finally, they were only studied the lines normal to the surface of the channel, vertical ones, but not in different angles. The uplift pressures generated by lines with different angles could be even higher than the studied ones. This fact makes the experimental results not conservative at all. Nowadays, there is still a potential need to analyze those cases. In the current project, those configurations will be simulated in order to understand the water behavior also for these geometries.

On the other hand, the report discussed about the possible effect of the boundary layer in the results, but there were no measurements related to it in the results neither analytical analysis of its conditions. However, the distance from the entrance of the channel to the location of the joint was so small that it was expected that the boundary layer was relatively thin in the tests and its effect was not significant. Also, there was no data neither about the flow depths, discharges and the slope of the channel. This suggests more accurate information for future researches on the field.

In the study, some conclusions where obtained:

1. The uplift pressures in the slabs increased when the horizontal gaps decreased. It can be explained because larger and stronger flow is circulating over the gap and part of its energy is dissipated as turbulence so that the generated uplift pressure is lower.

2. The uplift pressures increased when the vertical offset was higher. It is easy to understand with the boundary layer of the water flow. The velocity is higher when it is closer to the centerline of the channel, and as it is closer to the wall is going to zero. In this way, the higher is the vertical offset, the more it affects to the fluid with larger velocities. Small vertical displacements will just affect to the flow near the wall which has low velocity.

3. The velocity of the flow over the joints affects directly to the value of the dynamic pressure that was converted into static pressure. This effect was really small, but in most of the cases it was seen that for high velocities, the percentage of the velocity converted to uplift pressure was smaller.

1.5.2 Water tunnel tests (Frizell et. al, 2007)

This second study was carried out by the Bureau of Reclamation in 2007 by Warren K. Frizell in order to develop more accurately the previous research explained in the section above and obtain new results as well as new joint geometries effects. In this case, the study was made in a closed water tunnel. Even though it was not a true representation of the open channel flow, the main forces in this process are not the ones related to gravity, hence the depths of the flow are not the most important component. Consequently, the close conduit approximation could be applied obtaining valid results.

The experiment was done using a pump connected to the water tunnel in order to provide high velocities to the water. The flow that entered the test section was previously measured with a venturi meter and a mercury manometer. With the flow rate and the section of the area, the mean velocity of the channel could be obtained. In order to extract more accurate information about the velocity profile, a 2-dimensional particle image velocimetry (PIV) was set in the chamber near the joints. All the test layout is shown in the figure 5.

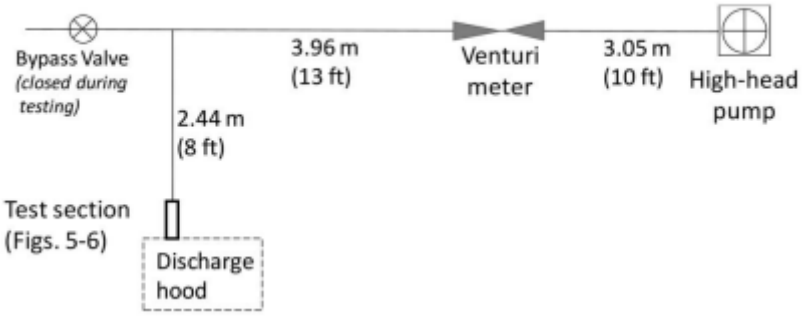

Figure 5-Layout of the test facility

The test chamber was 102 mm wide and 102 mm high. The water was pumped through a pipe 2.44 m long, where the first 0.91 m where a transition from 191mm diameter round pipe to a 102 mm square channel. The next 1.52 m where a square duct that was directly connected to the chamber shown in the figure 6.

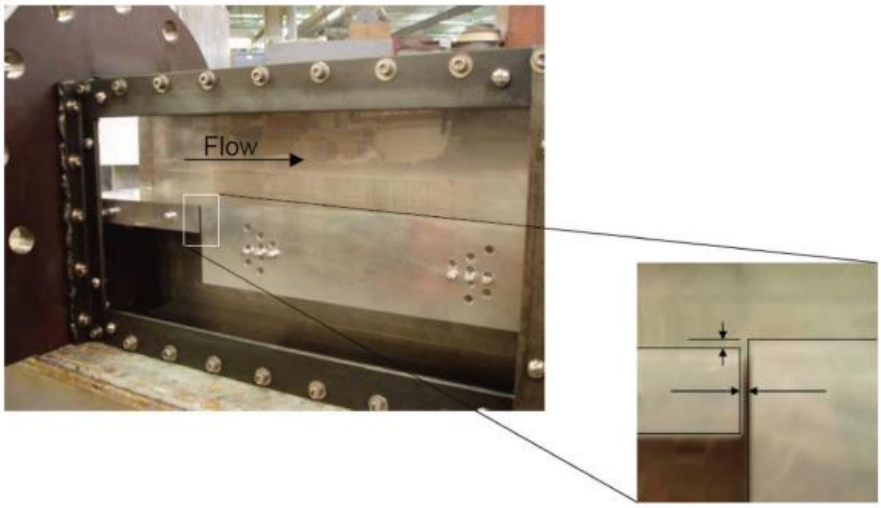

Figure 6-Water tunnel test chamber (Frizell, 2007)

In the chamber, a slot was formed in the tunnel between two plates to simulate a spillway joint which was adjusted to create offsets of 3.2, 6.4, 12.7 and 19.1 mm (1/8, 1/4, 1/2, and 3/4 in) and horizontal gaps of 3.2, 6.4, and 12.7 mm (1/8, 1/4, and 1/2 in). The flow entered a 102 mm square channel, and the outlet section was reduced from the nominal measure by the height of the offset. The flow left the chamber to atmospheric pressure. Figure 7 shows the test facility with all the measures of the water tunnel.

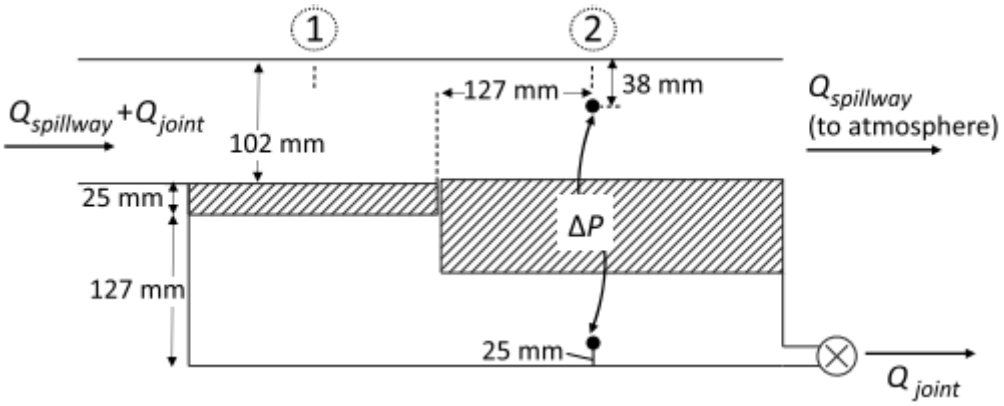

Figure 7 - Scheme of the test facility by Frizell, 2007

In this experiment, additionally to the rectangular sharp-edged joints (the one shown in the figure), also 45º chambered edges and radius edges were tested. Two set of tests were performed, first the sealed cavity was tested were there was no outflow under the slabs and Q_{joint} was equal to zero, and also the vented cavity was performed were there was a small quantity of fluid leaving the system through the joint. Although the size of the exit valve was not given in the report, it was not enough to vent all the chamber and as a result, there was a back-pressure below the slabs, even if it was not measured. The tests were done for velocities between the range of 5.2-14.6 m/s (17-48 ft/s).

In order to measure the uplift pressure in the slabs, two points were fixed below and above the movable block, and the differential pressure between those points was measured. However, there were some effects due to the water tunnel that distorted the results of the experiment. First, the difference in the tunnel height between the Section 1 and Section 2 due to the vertical offset produced a lower velocity upstream from the joint. This effect had a direct result of a higher pressure in this part of the facility than downstream the offset which would produce an alteration in the final results. Second, there was a pressure loss in the joints due to the contraction which would produce a lower pressure in the second section of the channel. Finally, the energy loss due to the friction during all the tunnel created and additional pressure difference between the two sections.

Other consideration that must be taken into account in the report is the effect of the boundary layer in the uplift pressure. In the experimental tests, the boundary layer velocity in the mid-height of the offset were around 70-90% of the mean velocity of the channel. In a prototype, it was expected to be below the 50% of the velocity. It means that the boundary layer velocities were not measured with exactitude which could increase the error in the results (Wahl, 2019).

Some of the conclusions made from this experiment were that in general, the uplift pressure increased with the velocity and the vertical offset height. Those values were higher in the sealed cavity tests than in the vented ones. However, the increase of the horizontal gap result generally in slight lower pressures. Comparing the results obtained with the different joints geometries, the chamber and radius edged cracks yielded results more similar to wider horizontal gaps of sharped edges. For example, a 1/4" sharp-edged gap present similar results to a 1/2” radius or chamber edged gaps.

1.6 Purpose and goal

The aim of this Master Thesis is to write out a study, in collaboration with Vattenfall R&D in Älvkarleby, that examines flow velocity and hydro-dynamic pressure conditions, which are affected by a combination of geometrical parameters at the joints in order to carry out a correct design and prevent this type of accident from happening again.

The study will be based on previous laboratory studies e.g. by Bureau of Reclamation, and recent findings in the subject area. Regarding the simulations of the model, Ansys Fluent 2022 R1 will be used during the project as the main tool.

Moreover, it is expected to improve the knowledge of CFD modelling, including the geometry, the mesh generation, the set-up of the model and boundary conditions. Also, learning about turbulence models that are used in the program and the differences between them. Finally, it is expected to learn a general knowledge about the hydropower plants, and the security of the different components of them.

1.7 Limitations

The main objective of this project is to carry out a numerical analysis of the uplift pressures generated under the slabs due to the high velocities, and also compare the results to the experimental results obtained by Frizell in 2007 in his study. For this purpose, a CFD geometry similar to the experimental model used in the mentioned study is going to be created in order to obtain the most accurate results possible. However, one of the major limitations of this project is the lack of information regarding the dimensions of the test model, as well as the profile of water velocities and pressures. Therefore, due to this lack of data, it is expected to obtain results with a significant margin of error but which conform to the patterns obtained in the experimental results.

2 Theory

2.1 Equations of fluid dynamics

In this section, the theory necessary to understand the equations that govern the fluid dynamics will be explained and the considerations that the CFD software takes into account in order to carry out the simulations. Likewise, the different existing turbulence models will be explained in order to understand which is the most suitable model for the present project.

2.1.1 Stagnation pressure phenomena

To properly understand the phenomenon that will be the basis of this project, it is important to first introduce the meaning of the stagnation pressure that can be clearly explained with the Bernoulli and steady-flow energy equations.

Considering a fluid particle in constant motion and with negligible viscosity and applying the Newton's second law in the direction of the flow, the next equation is obtained which relates the change in the speed, the pressure gradient and the height of the particle:

$$\frac{1}{2}d(V^2) + \frac{dP}{\rho} + gdz = 0 \qquad (1)$$

where,

ρ = fluid density

P = fluid pressure

V = fluid velocity

g = gravitational acceleration

z = elevation

Considering that the fluid is incompressible and analyzing the equation above between two points of the streamline, it results in:

$$\frac{{V_1}^2}{2g} + \frac{P_1}{\rho g} + z_1 = \frac{{V_2}^2}{2g} + \frac{P_2}{\rho g} + z_2 \qquad (2)$$

The first term of the equation is considered the dynamic pressure, and it is the pressure related to the velocity of the fluid. The second and third terms together make up the static pressure of the fluid which depends on the specific weight and its height. This equation can be used when the total energy is conservative between the two points. However, if there are any pressure losses due to the friction or other external factor, it would directly affect to the energy of the flow and a new term should be added to the equation referring to these losses.

In this way, the stagnation pressure of a fluid is defined as the static pressure of a fluid when its velocity is zero. Applying the Bernoulli's equation between two points at the same height and considering no energy losses, the stagnation pressure related to a fluid with a certain velocity would be defined as following:

$$\frac{{V_1}^2}{2}\rho = P_2 - P_1 \qquad (3)$$

This physical phenomenon can lead to high pressures at stagnation points of a fluid when it reaches high velocities like in the study case of the current project (Vakil & Green, 2011)

2.1.2 Navier-Stokes equations

The next part of the study will be carried out with two fluids, water and air. Both are Newtonian fluids that follow Newton's viscosity laws, which means that the viscosity of these fluids is only dependent on temperature and pressure. Newton's viscosity law can be seen in the following formula (Yang, Teng & Lin, 2019),

$$\tau = \mu \frac{du}{dy'} \qquad (4)$$

where,

τ = Shear stress $[N/m^2]$

μ = dynamic viscosity $[Ns/m^2]$

du/dy' = shear rate $[s^{-1}]$

As mentioned above, the fluids simulated in the project are Newtonian fluid and therefore, can be described by Navier-Stokes equations. Those equations include the continuity equation and the momentum equation which are shown in (5) and (6) respectively,

$$\frac{\partial \rho}{\partial t} + \nabla(\rho v) = 0 \qquad (5)$$

$$\rho \frac{\partial v}{\partial t} = \rho \left[\frac{\partial v}{\partial t} + (v \cdot \nabla)v\right] = -\nabla p + \rho g + \mu \nabla^2 v + (\mu + b)\nabla(\nabla \cdot v) \qquad (6)$$

$v =$ Velocity $[m/s]$

t = Time $[s]$

p = Pressure $[N/m^2]$

b = Second coefficient of viscosity $[Ns/m^2]$

However, it is impossible to find solutions to the Navier-Stokes equations analytically, so that it is necessary to make some simplifications. In the case study of this project, the flow will be considered as steady state flow, and the working fluids will be incompressible. If the fluid is taken as incompressible the velocity divergence is equal to zero as it is shown in the next equation.

$$\nabla \cdot v = 0 \qquad (7)$$

The Navier-Stokes equations take then the following simplified form, which is useful for incompressible flows.

$$\rho \frac{\partial v}{\partial t} = \rho \left[\frac{\partial v}{\partial t} + (v \cdot \nabla)v\right] = -\nabla p + \rho g + \mu \nabla^2 v \qquad (8)$$

2.1.3 Turbulence models

When doing the simulation in the CFD, it is really important the choice of the turbulent model as it describes the turbulent properties of the fluid and it can change depending on the case and simulating model (Shaymaa & Alhashimi, 2022).

In order to analyse the turbulence of a model it can be done by a direct numerical simulation, DNS, which normally is not common as it requires great computational calculations and it gives results that are not necessary. Other alternative is to base the analysis in the Reynolds Averaged Navier-Stokes equations (RANS). These equations consider that all turbulent flow are composed by a mean component and a turbulent component in order to define each instantaneous value. The equation is written as follows,

$$\frac{\partial U_i}{\partial t} + U_j \frac{\partial U_i}{\partial x_j} + \frac{\partial u_i u_j}{\partial x_j} = -\frac{1}{\rho}\frac{\partial p}{\partial x_i} + v\frac{\partial^2 U_i}{\partial x^2{}_j} \qquad (9)$$

where,

U_i = mean (time-averaged) velocity in the i direction

x = position

u = fluctuating velocity in i and j directions

The equation above can be rewritten as,

$$\frac{\partial U_i}{\partial t} + \rho U_j \frac{\partial U_i}{\partial x_j} = -\frac{\partial}{\partial x_j}\left[p\delta_{ij} + \mu\left(\frac{\partial U_i}{\partial x_j} + \frac{\partial U_j}{\partial x_i}\right) - \rho u_i u_j\right] \qquad (10)$$

There are some new terms that appear in this equation and need to be solved in order to obtain accurate results. The term $-\rho u_i u_j$ is called the Reynolds stress tensor, and the δ_{ij} is the Kronecker delta and it is 1 if i=j and zero in any other case. In order to model the Reynolds stresses, the Boussinesq hypothesis must be introduced which links the correlations with the velocity components.

$$-\rho u_i u_j = \mu_t\left(\frac{\partial U_i}{\partial x_j} + \frac{\partial U_j}{\partial x_i}\right) - \frac{2}{3}\delta_{ij}\rho k \qquad (11)$$

where k is the turbulent kinetic energy per unit mass and μ_t is the turbulent viscosity. This last term is not a property of the fluid but it is related to the dynamic characteristics of the flow. In this way, different first order models are presented which are based on the dynamical characteristics of the flow in order to model the turbulent kinetic of the flow.

2.1.3.1 Standard k-ε model

The standard k- ε model is one of the most common models used in CFD. It is widely used among engineers as it provides results within a wide range, and with reasonable accuracy. It has been previously used in numerous simulations related to flows around different elements and analysis of drag and lifting forces providing exact results (Wang et. al, 2019).

In this model, the ε represents the dissipation rate of the turbulent kinetic energy and it affects directly to the way the turbulence is interpreted. There is not an exact transport equation but some approximations are needed in order to solve the problem. The following equations represent the transport equations for k and for ε respectively.

$$U_i \frac{\partial k}{\partial x_i} = \frac{1}{\rho} \frac{\partial}{\partial x_i} \left(\frac{\mu_t}{\sigma_k} \frac{\partial k}{\partial x_i} \right) + P_k - \varepsilon \tag{12}$$

$$U_i \frac{\partial \varepsilon}{\partial x_i} = \frac{1}{\rho} \frac{\partial}{\partial x_i} \left(\frac{\mu_t}{\sigma_\varepsilon} \frac{\partial \varepsilon}{\partial x_i} \right) + c_1 \frac{\varepsilon}{k} P_k - c_2 \frac{\varepsilon^2}{k} \tag{13}$$

In those equations, new variables are introduced, the P_k respresents the production rate of turbulent energy and is calculated as follows, while the new constants have the values shown in the table.

$$P_k = \frac{\mu_t}{\rho} \left(\frac{\partial U_i}{\partial x_j} + \frac{\partial U_j}{\partial x_i} \right) \frac{\partial U_i}{\partial x_j} \tag{14}$$

Table 1 - Constants of the standard k-ε turbulence model

Constant	c_μ	c_1	c_2	σ_k	σ_ε
Value	0.09	1.44	1.92	1.0	1.3

2.1.3.2 Shear-stress turbulent (SST) k- ω model

The turbulence model explained in the section below has some difficulties to specify the dissipation rate (ε) when the fluid is near the wall. In this way, this new model tries to overcome this difficulty introducing the transport equation of the specific dissipation rate (ω) instead of the dissipation rate. The equations for this model are the following ones for k and ω respectively.

$$\rho U_i \frac{\partial k}{\partial x_i} = \frac{\partial}{\partial x_j}\left((\mu + \frac{\mu_t}{\sigma_k})\frac{\partial k}{\partial x_j}\right) + G_k - Y_k + S_k \tag{15}$$

$$\rho U_i \frac{\partial \omega}{\partial x_i} = \frac{\partial}{\partial x_j}\left((\mu + \frac{\mu_t}{\sigma_\omega})\frac{\partial \omega}{\partial x_j}\right) + G_\omega - Y_\omega + S_\omega + D_\omega \tag{16}$$

Where G_k is the generation of the turbulence kinetic energy due to the mean velocity gradient, G_ω is the generation of ω. Y_k and Y_ω are the dissipation of each parameter due to the tubulence, D_ω is the cross-diffusion term and S_ω and S_k are user defined source terms (Kocaer & Yarar, 2020).

2.1.4 Multiphase flow

According to Song and Zhou (1999), it is very common to find in the nature a flow that consist in different phases. This kind of flow are called multiphase flows and there is a special tool in Ansys in order to simulate them. In the current project a free-surface water flow has been studied, which means that the water was flowing surrounded by air. In order to correctly simulate it in Ansys, the Euler-Euler method has been used. With this approach, three different models could be chosen, the Volume of Fluid, the Mixture model and the Eulerian model. The most suitable one for the purpose of the current study was the Volume of Fluid as it is a surface tracking model, and is the most suitable for working with free surfaces (Song & Zhou, 1999).

2.1.5 Volume of fluid (VOF)

The volume of fluid (VOF) is a method commonly used in the CFD in order to work with fluids composed by two or more phases. One of the main restrictions of this model is that phases must be immiscible between them, but the parameters of the fluid will be common for the mixture. This model is widely used in free-surface flow for example, where there is a mixture of air and water in the working fluid (Bayon et. al, 2018). Each phase takes a volume fraction that must sum the unity, and it is mathematically expressed as follows,

$$\sum_{q=1}^{n} \alpha_q = 1 \tag{17}$$

The properties of the materials are stated by the addition of the properties of each of the phases multiplied by the ratio of it. For example, for the case of the density, it would be calculated as follows.

$$\sum_{q=1}^{n} \alpha_q \rho_q = \rho \tag{18}$$

Finally, the momentum equation for each of the phases must be solved as follows,

$$\frac{1}{\rho_q}\left[\frac{\partial}{\partial t}\alpha_q \rho_q + \nabla \cdot \left(\alpha_q \rho_q v_q\right) = S_{\alpha_q} + \sum_{p=1}^{n} (\dot{m}_{pq} - \dot{m}_{qp})\right] \tag{19}$$

3 Method

In the next section the methodology followed in order to carry out the study will be explained. Figure 8 shows a brief outline of the steps that have been taken during the process. First of all, the geometry that was used in the simulations was created. Then, the mesh to work with was generated and it was set up by introducing all the data of the problem, such as the boundary conditions, the turbulence model, the multiphase model, etc. Once the setting up was done, the simulation has been run and the program presented some results. These results were analyzed to check if there was mesh independence and the system converges (these terms will be explained in more detail later). Once the results have been checked to be reliable, they were compared with the experimental data in order to verify that they were correct. All this process has been done with Ansys Fluent 2022 R1.

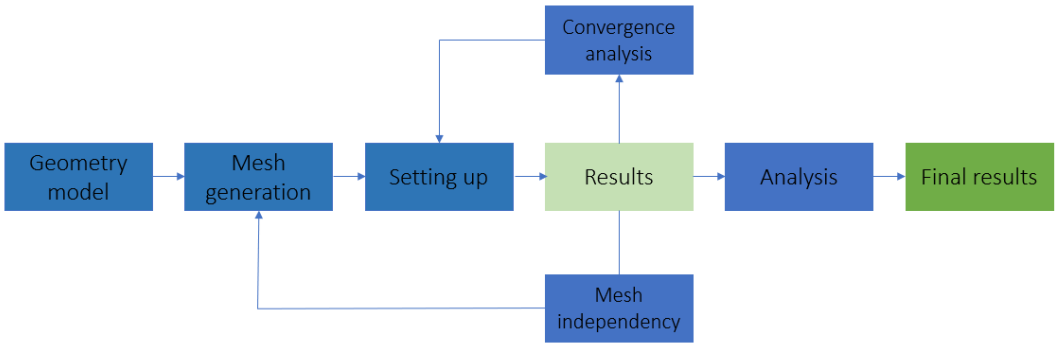

FIGURE 8 - METHODOLGY SCHEME OF THE WORK PROCESS

As explained before, the study was divided into two main parts. In the first, the model stated by Frizell (2019) was built in order to analyze it in the CFD and compare the numerical results to the experimental ones obtained in the tests. For the second part, a second set of configurations were simulated for open channel, with new characteristics as it will be shown later. It was used the same model that was previously checked with the experiments, so that it was not necessary to study the mesh independency. However, the introduction of the free-surface resulted in convergence difficulties when running the simulation. For this reason, a convergence analysis was necessary previous to the simulation in order to obtain accurate results in the end.

3.1 Geometry

In order to build the geometry, *Spaceclaim* 2022 R1 was used which is a part of the Ansys simulation software package. This tool works with 2D and 3D models, allowing you to define the geometries that will later be meshed and analyzed. In the current project, the geometry was previously defined in the study done by Frizell that has been previously shown in figure 7. Thus, *Spaceclaim* has been used to model the same geometry as shown in the figure below.

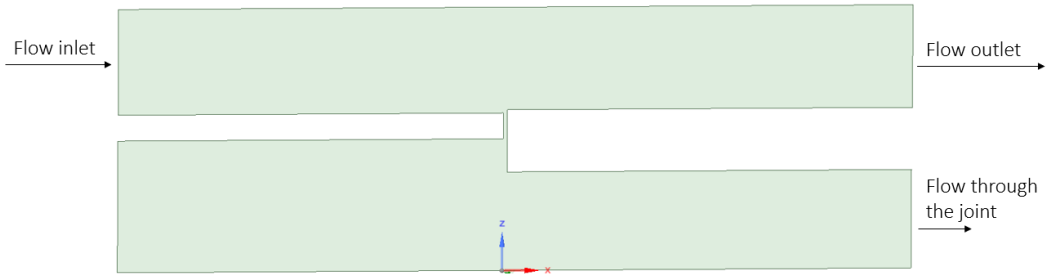

FIGURE 9-SPACECLAIM GEOMETRY OF THE TESTS SECTION FOR CFD MODELLING

The flow inlet line is 102 mm high, and it was set for all the simulations. The heigh of the slab upstream the joint is 25 mm as stated in the experimental test, but there was no data about the height of the slabs downstream the crack so a starting height of 60 mm was set, which has been changing depending on the geometries that were simulated. Also, the outlet flow line took different values depending on the test conditions. Finally, the gap under the slabs where the uplift pressure was to be measured had a deep of 127 mm under the first slab and 95 mm in the joint outlet part. In total, the section of the tunnel had an horizontal lenght of 785 mm. Althought this measure was not stated in the experiment report, different lenght have been simulated in order to find the most accurate results avoiding errors due to the boundary layer development and the outlet atmospheric pressure affecting the results.

The geometry was set so that the floor of the tunnel was in the x-axis and the flow through the tunnel was in the positive direction of it. The gravity was applied in the z-axis downwards, and the y-axis was perpendicular to the plane but as the model was built in 2D, the last one was innecesary. The origin of the coordinate axis system was set in the bottom of the tunnel down the slabs for the z-axis. For the x-axis, it was located in the starting line of the joint/crack. Both positions were situated in purpose in order to make it easier the pressure points measurements later.

The figure 9 shows the geometry built for the sharp-edged joint configurations, more exactly for the 1/8-inch offset 1/8-inch horizontal gap configuration- However, different models were built in order to simulated the chamber-edged, and radius-edged configurations, they are shown in the following figures respectively.

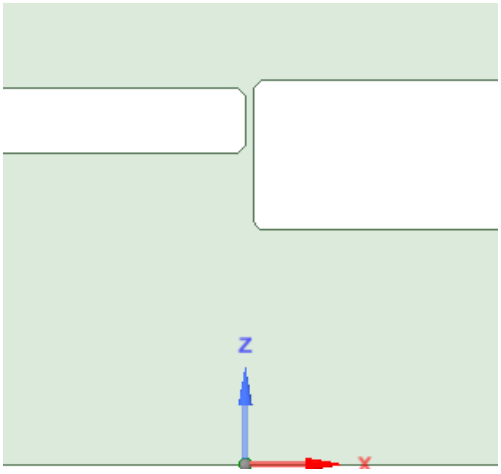

FIGURE 10-SPACECLAIM GEOMETRY FOR CHAMBER-EDGED CONFIGURATION

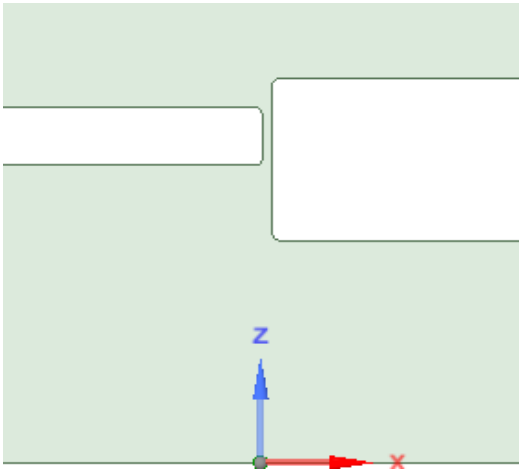

FIGURE 11-SPACECLAIM GEOMETRY FOR RADIUS-EDGED CONFIGURATION

In the second part of the study, an angle was set for the water tunnel in order to analyze the effect of the gravity in the water behavior. The new geometry is shown in the next figure, where alfa took values of 30º and 45º for the simulations. For these cases only the sharp-edged 1/8-inch offset 1/8-inch gap configurations were studied for the sealed cavities. In this case the height of the chamber was increased 50 mm in order to be able to determine clearly the free-surface in the simulations.

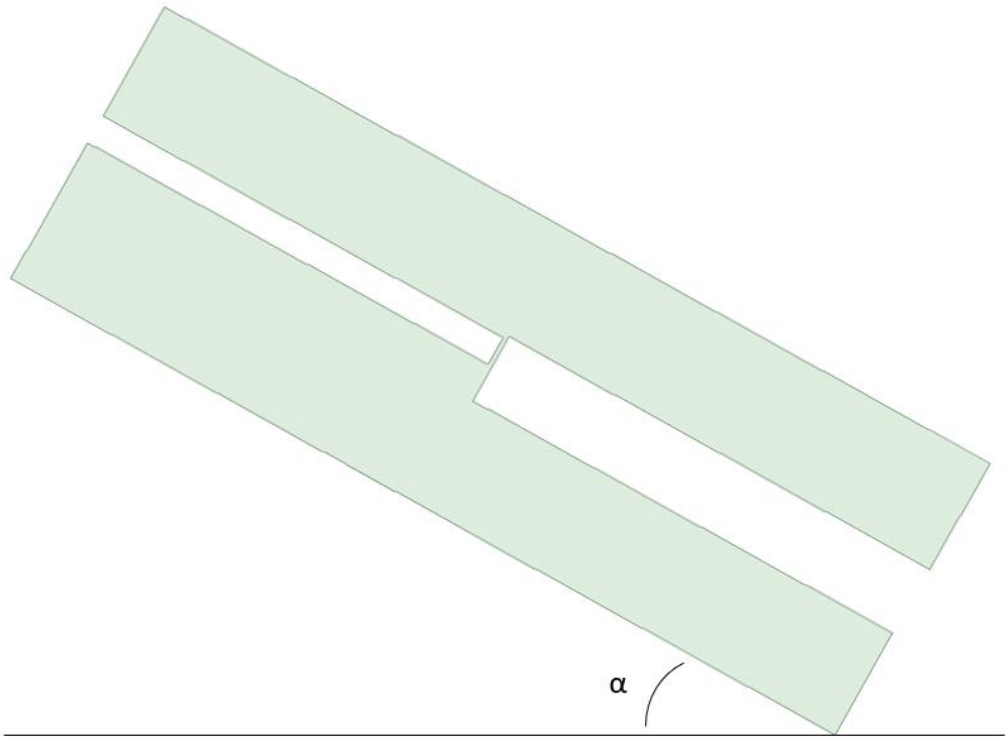

FIGURE 12-SPACECLAIM GEOMETRY FOR SLOPE CONFIGURATION

3.2 Mesh quality

All the mesh of the geometry was built in the Ansys, no external tools where needed. Due to the characteristics of the geometry, and the fact that the model was built in 2D, only quadrilateral and triangular elements were needed in order to compose all the mesh. The edge sizing tool has been used in the walls of the tunnel in order to have more accurate analysis of these parts of the channel avoiding too much computational power in analyzing all the mesh with this accuracy. In the next figure it is shown the mesh of the 1/8-inch 1/8-inch sharp-edged geometry, the rest of the geometries had the same meshing structure but just the geometry changed.

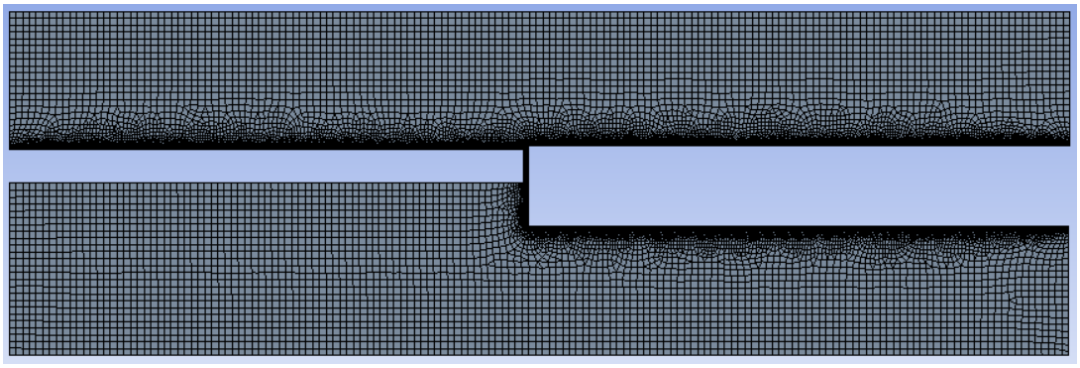

FIGURE 13-ALL THE GEOMETRY MESHED

One of the most important aspects of the meshing is to obtain accurate results and avoid the mesh dependency on the analysis. For this reason, a mesh dependency study has been made in order to analyze the accuracy of the results in each configuration. In the next figure it is shown the precision of the results obtained for three mesh configurations. The last two cases provided faster simulations but resulted in larger errors compared to the experimental results. It is why, it was decided to build the mesh with a 5 mm of size in the mean elements and 0.5 mm in the edges that provides and acceptable error of 4%.

Table 2 - Mesh independency study

Mesh independence study		
Mean element size	Edge sizing	Error %
0,005	0,0005	4%
0,005	0,0007	7%
0,01	0,005	8%

Finally, for studying the quality of the mesh it is analyzed the skewness of the elements. In this case, the maximum skewness value obtained was 0.68902 while the mean skewness value was 0.12462, which are assumed to be considerable good results. Those results were obtained for the case shown in the figure 9. Different geometries would result in little variations of those values but still in the range of optimal quality of the mesh.

For the second model with the slope and open channel, the same mesh was used but the elements in the upper side of the tunnel was set to 0.5 mm as well as the edges in order to analyze more accurately the edge of the water in contact with the air.

3.3 Ansys fluent

Apart from the previously explained conditions related to the boundary and the turbulence model, other setup conditions have been configured in the model in order to correctly run the simulations. The model has been created in a 2D double precision pressure-based SIMPLE scheme. The operating pressure was set to atmospheric pressure, 101325 Pa and the gravity acceleration was set to -9.8 m/s^2 downwards in the Y direction. The VOF volume was set with two Eulerian phases for the water and the air and the explicit formulation. The volume fraction cutoff was left in $1 \cdot 10^{-6}$ as a default value.

Finally, the iteration process was initialized with 0.01 seconds as the time step size with a maximum number of iterations of 20 per time step. These conditions were used for the close channel tunnel as there was not needed a large computational time for converging the results. In the case of the free-surface simulations with slopes, more computational power was needed and initial time step size of 0.0001 seconds was set. Additionally, the simulation was run firstly as a close channel with a wall as a boundary condition in the top of the chamber until the simulation reached the convergence. Once the results were established, the upper boundary condition was changed to inlet pressure in order to avoid convergence problems.

3.4 Boundary conditions

When setting up the model in CFD, it is important to set the boundary conditions correctly, because if they are wrong, the results will not be trustable. There are many conditions that can be changed, such us the inlet flow, the outlet, the walls or the free-surface.

Regarding the inlet flow, it is usual to use the velocity or the pressure inlet condition. However, those methods are more used for incompressible flows, when working with a compressible fluid, a mass flow inlet condition is commonly applied. Related to the outlet conditions, a pressure condition is recommended when the outlet pressure is known as it gives better convergence rate. In any other case, the outflow boundary condition can be used when the outflow profile is unknown, but is not recommended for compressible flows. Finally, the conditions applied in the walls are important, which is a no-slip condition by default, but it can be changed and set the wall roughness.

Previous researches have analyzed the most accurate boundary conditions for the study of the water flow over a spillway. In the first part of the study, as it was analyzed a water tunnel, wall condition was set to all the edges of the tunnel. For the outlet of the fluid atmospheric pressure was set and the velocity inlet was also known. In the case of the vented configurations, a small gap was built down the slab, and the discharge mass flow rate was set for each case. This data was taken from the graphics shown in the experimental report.

In the second part of the study, an open channel was analyzed with a certain slope. For this reason, the atmospheric pressure was set in the upper border of the model as an inlet pressure.

3.5 Turbulence model analysis

The correct choice of the turbulence model has a big effect in the obtained results as it describes the turbulence properties of the fluid. Therefore, a previous study of the turbulence model accuracy has been done in order to analyze which method would represent more precisely the model and the case study.

With this purpose, the sharp-edged geometry with 1/8-inch offset and 1/8-inch gap for sealed cavity has been chosen in order to analyze the turbulent model effect on the results. Taking into account previous researches on the field, and due to the characteristics of the current study, it has been decided to analyze the next three models, the Standard k- ε, the Standard k- ω and the SST k- ω. Table 3 shows the results obtained with each of them.

Table 3 - Comparation of the results obtained for different turbulence models

Turbulence model	Uplift Pressure (Pa)		
	Experimental	Numerical	Deviation (%)
Standard k-ϵ		49362,20	-5%
Standard k-ω	51631,72	56438,13	9%
SST k-ω		54668,98	6%

Regarding the time needed for completing the simulations, no big differences have been observed between the different models as the simulations converged in a really short time. It can be due to the geometry and the fact that the model was built in 2D that it did not need excessive time to obtain the results. Anyway, for further simulations in 3D with more complex models, the running time could be a determinant factor that could have an effect in the turbulence model choice.

On the other hand, looking at the results obtained in table 3, both the Standard k-ε model and the SST k-ω model gave accurate results. However, taking into account the values obtained for the vented cavities, the Standard k-ε model provided more exact results in both cases.

4 Results

In this section, the results obtained from the simulations will be explained and compared to the experimental data from the report. Some of the cases tested in the experiments have been simulated for both vented and sealed cases for different configurations. The uplift pressures will be analyzed for three velocities, 50, 70 and 90 ft/s (15.24, 21.34 and 27.43 m/s).

4.1 Closed channel simulations

For the water tunnel tests comparation, a closed channel has been simulated for different configurations and geometries. One configuration has been modeled for each edge geometry, and both vented and unvented cases have been simulated and compared. The pressure difference has been taken from two points under and above the slab downstream the joint, as it is stated in the experimental report. The points were 0.127 m downstream the crack. The points were situated 0.025 and 0.216 m from the bottom of the chamber.

4.1.1 Sharp-edged geometry

For the sharp-edged geometry, 1/8-inch offset (3.2 mm) and 1/4-inch (6.4 mm) gap cavity has been simulated for the three velocities. In the table 4 the results obtained for the sealed configuration are shown. It can be seen that the accuracy presented by the numerical simulations are lower than 5% of a deviation related to the experimental data, which means that the numerical model has a high exactitude.

Table 4 - Experimental and simulated uplift pressure, sharp-edged geometry, 1/8-inch offset, 1/4-inch gap, sealed cavity (Frizell, 2019)

Velocity (ft/s)	Uplift Pressure (Pa)		
	Experimental	Numerical	Deviation (%)
50	41043.54	43389.38	5%
70	82494.31	84853.78	3%
90	138954.14	141031.37	1%

In the table 5, the uplift pressures for the vented configuration are shown for the three velocities. In this case, the range of deviation has increased related to the sealed configurations taking values of around 15%, moreover, the uplift pressure value has remained almost constant in both cases, being the experimental value the one that has decreased in a larger percentage.

Table 5 - Experimental and simulated uplift pressure, sharp-edged geometry, 1/8-inch offset, 1/4-inch gap, vented cavity (Frizell, 2019)

Velocity (ft/s)	Uplift Pressure (Pa)		
	Experimental	Numerical	Deviation (%)
50	35911.83	42127.94	15%
70	73132.9	83047.97	12%
90	124398.38	138691.41	10%

The water behavior through the chamber is shown in figures 14, 15 and 16 for sealed geometries with a flow velocity of 50 ft/s (21,34 m/s). The velocity in the CFD-post is given in m/s and the pressure in Pa. The stagnation phenomena can be easily demonstrated in figure 14 where the water that comes into the joint losses its velocities ending up in values around 0 m/s. A little turbulence is generated over the joint. The velocity difference before and after the joint over the channel in figure 16 can be explained as a result of the contraction of the channel in order to generate the joints offset. This velocity difference increases as the joint offset becomes higher.

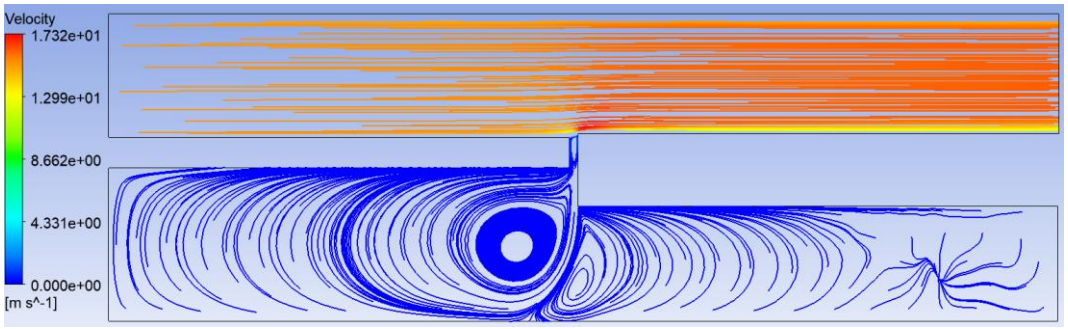

Figure 14-Velocity streamlines through the chamber for 50 ft/s in sharped-edged sealed geomtry

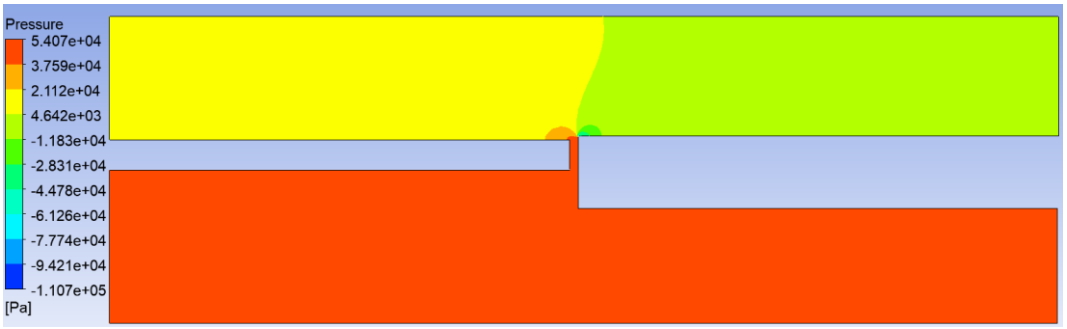

Figure 15-Pressure [Pa] distribution through the chamber for 50 ft/s in sharped-edged sealed geomtry

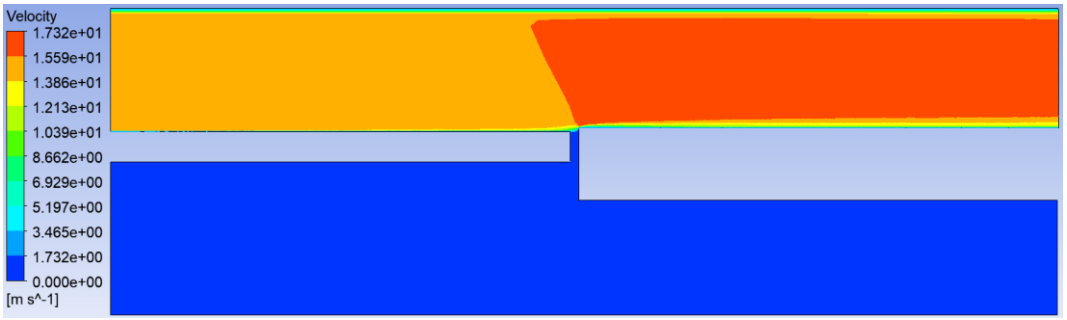

Figure 16-Velocity [m/s] profile of the flow through the chamber for 50 ft/s in sharped-edged sealed geomtry

In figure 17, the velocity streamlines are shown for vented cavity where it can be appreciated the more amount of water flowing through the joint compared to the unvented cavity. It is due to the discharge under the slabs that generates more water movement in the cavity.

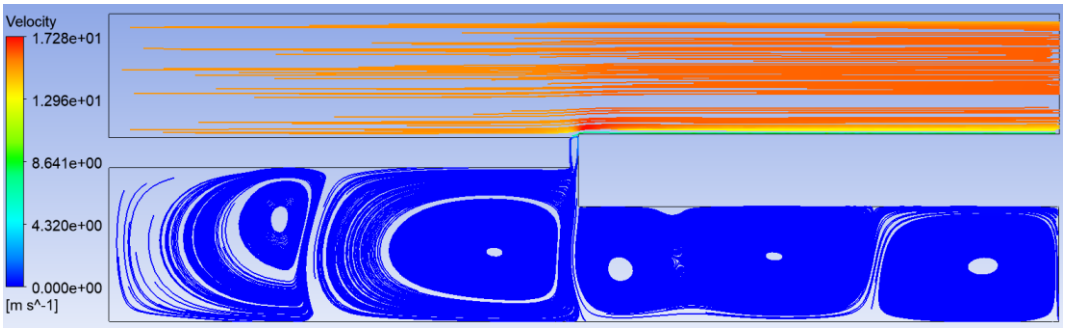

Figure 17 - Velocity streamline through the chamber for 50 ft/s in sharped-edged vented geomtry

The water velocity and pressure profiles for vented geometries follows the same pattern as in sealed cavity cases.

4.1.2 Chamfer-edged geometry

For the chamfer-edged analysis, the 1/4-inch offset (6.4 mm) 1/8-inch (3.2 mm) gap configuration has been simulated. The presented results shows that the accuracy of the model for the chamfer-edged case with sealed cavity is high, obtaining values of 6% of deviation between the experimental tests and the numerical results. It has been also observed in this case that the numerical value obtained are lower than the experimental ones.

Table 6- Experimental and simulated uplift pressure, chamfer-edge geometry, 1/4-inch offset, 1/8-inch gap, sealed cavity (Frizell, 2019).

Velocity (ft/s)	Uplift Pressure (Pa)		
	Experimental	Numerical	Deviation (%)
50	65369.76	62253.42	5%
70	129847.27	122456.13	6%
90	216797.23	203983.91	6%

In the second case, for the vented configuration it is shown in the next table that the deviations from the experimental cases are similar to the previous ones. It can be observed that the numerical values have remain almost constant in comparation to the decrease that has develop the pressure in the experimental tests, however, the deviation seems to keep constant. It is due to the fact that in the unvented cases, the numerical values where 5% under the experimental value. In this second cases, the numeral values are around 5% above the experiments.

Table 7 - Experimental and simulated uplift pressure, chamfer-edge geometry, 1/4-inch offset, 1/8-inch gap, vented cavity (Frizell,2019).

Velocity (ft/s)	Uplift Pressure (Pa)		
	Experimental	Numerical	Deviation (%)
50	58708.38	62499.62	6%
70	117290.69	122856.88	5%
90	196678.7	204627.67	4%

In figures 18, 19 and 20 the velocity streamlines, the pressure distribution and the flow velocity through the channel are shown respectively for sealed geometries and 50 ft/s (21,34 m/s) mean flow velocity. In figure 20, it can be observed the turbulences generated due to the joints. There is a velocity increase directly after the crack, while a decrease in the flow velocity is appreciated just before the joint due to the water stagnation.

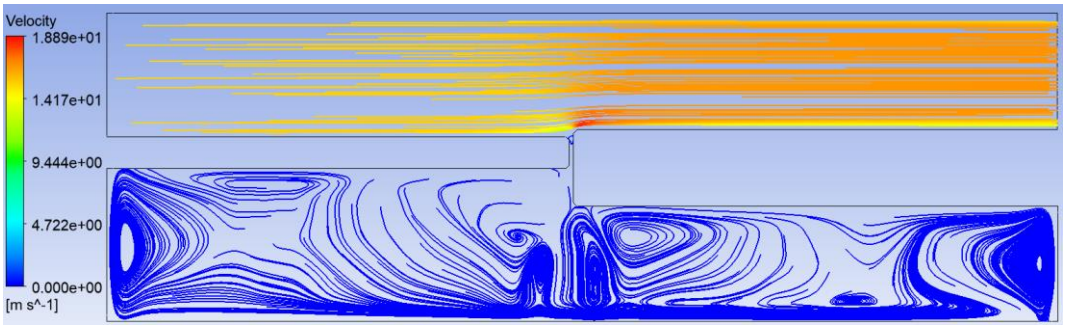

Figure 18 - Velocity streamlines through the chamber for 50 ft/s in chamfer-edged sealed geomtry

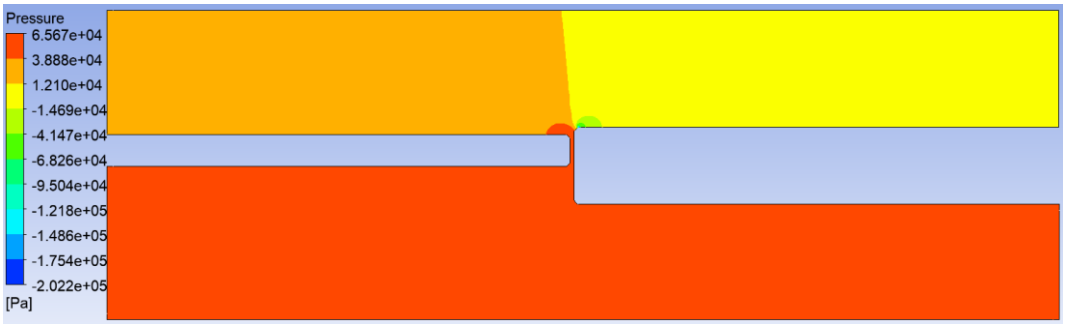

Figure 19 – Pressure [Pa] distribution of the flow through the chamber for 50 ft/s in chamfer-edged sealed geomtry

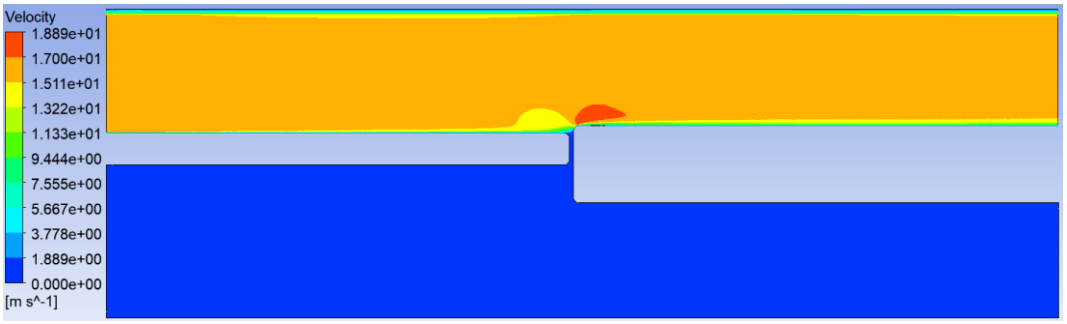

Figure 20- Velocity [m/s] profile of the flow through the chamber for 50 ft/s in chamfer-edged sealed geomtry

The streamlines for the vented geometry are shown in figure 21. It is observed how there is more water flowing through the joint to the cavity when there is a little discharge.

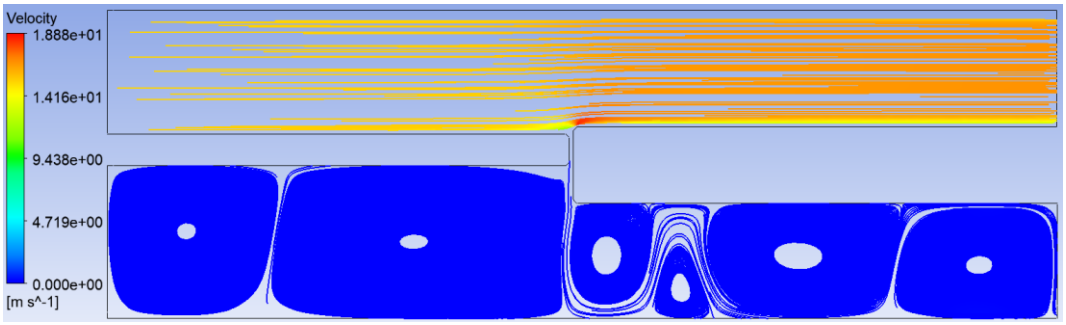

Figure 21 - Velocity streamlines through the chamber for 50 ft/s in chamfer-edged vented geomtry

4.1.3 Radius-edged geometry

In the last case, it has been studied the model of 1/8-inch offset (3.2 mm) and 1/8-inch (3.2 mm) gap. The results obtained in this model shows the similar deviations to the other ones, taking values of around 3%.

Table 8 - Experimental and simulated uplift pressure, radius-edged geometry, 1/2-inch offset, 1/8-inch gap, sealed cavity (Frizell, 2019)

Velocity (ft/s)	Uplift Pressure (Pa)		
	Experimental	Numerical	Deviation (%)
50	45105.66	46704.13	3%
70	89548.34	92172.55	3%
90	149453.84	154179.84	3%

For the vented cases, the deviation has increase until values of 10%, which means an increase of around 7% from the sealed cavity geometries.

Table 9 - Experimental and simulated uplift pressure, radius-edged geometry, 1/2-inch offset, 1/8-inch gap, sealed cavity (Frizell, 2019)

Velocity (ft/s)	Uplift Pressure (Pa)		
	Experimental	Numerical	Deviation (%)
50	40822.93	45469.22	10%
70	82421.12	90863.97	9%
90	139298.4	153152.21	9%

In figures 22, 23 and 24 the velocity streamlines, the pressure distribution and the velocity of the flow through the channel are shown respectively for sealed cavity cases and 50 ft/s (21,34 m/s) flow mean velocity.

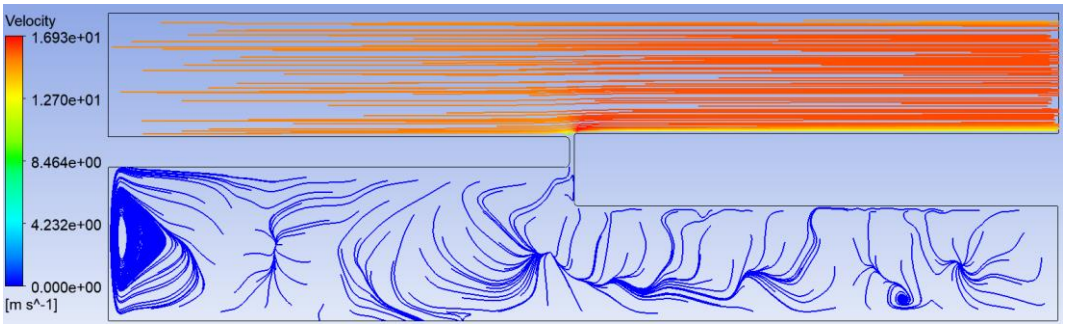

Figure 22-Velocity streamlines through the chamber for 50 ft/s in radius-edged sealed geomtry

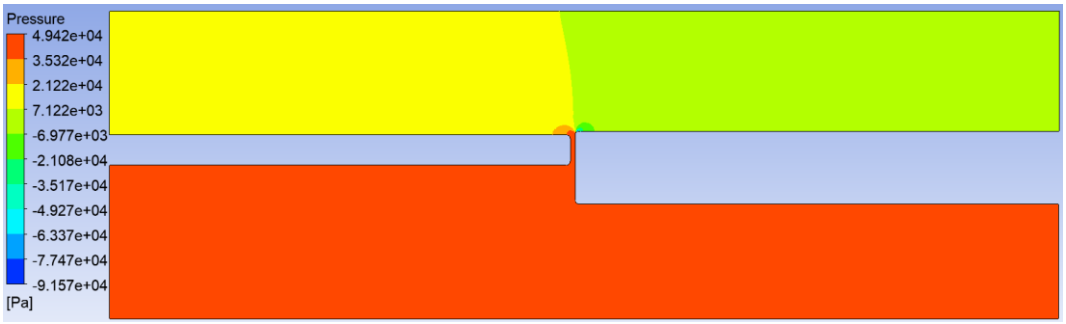

Figure 23 - Pressure [Pa] distribution of the flow through the chamber for 50 ft/s in radius-edged sealed geomtry

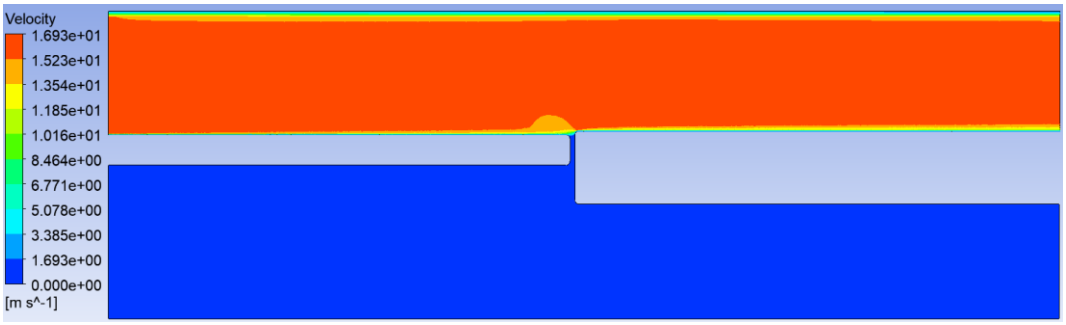

Figure 24- Velocity [m/s] profile of the flow through the chamber for 50 ft/s in Radius-edged sealed geomtry

In figure 24 the velocity streamlines are shown for the vented geometry for a mean flow of the channel of 50 ft/s (21,34 m/s).

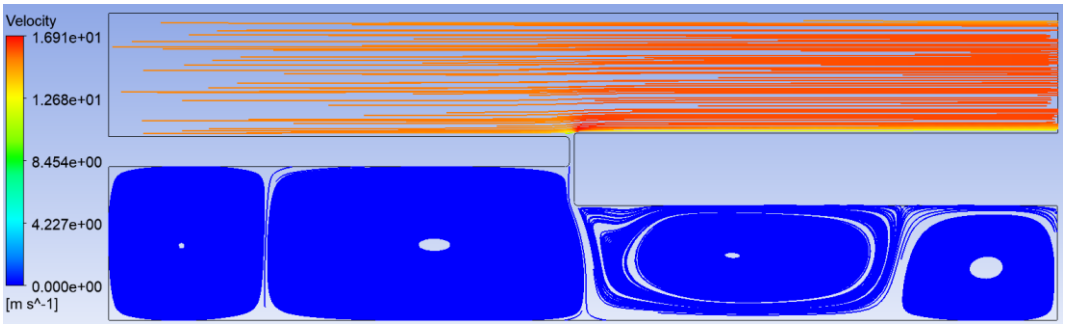

Figure 25- Velocity streamlines through the chamber for 50 ft/s in radius-edged vented geomtry

In general terms, the three cases present great exactitude related to the experimental tests, and follow the same patterns. However, in all of them there is a higher deviation due to the discharge flow rate of the cavity.

4.2 Open channel simulations

For open channel geometries two slopes have been simulated, the flow over a 30º and 45º chutes. For these tests, the sharp-edged sealed geometry has been chosen with a joint gap of 1/8-inch (3.2 mm) length and an offset 1/8-inch (3.2 mm) high. The simulations have been made for the three velocities tested before, 50, 70 and 90 ft/s (15.24, 21.34 and 27.43 m/s). The height of the channel has been increased 50 mm in order to observe the free surface of the flow.

For easier understanding of the results, the figures are presented horizontal even if they have been modeled with different slopes.

4.2.1 Slope of 30º

In this section, the results obtained for the water profile in a 30º inclination chamber are presented. The figures correspond to the 50 ft/s (21,34 m/s) flow velocity simulations. In figure 26, the pressure distribution among the chamber is shown. It is seen that above the slabs the pressure is near to the atmospheric pressure as a free-surface has been applied, while high pressures are generated under the joint. The uplift pressure takes values of around 41000 Pa which is a little bit lower than the close channel horizontal measured values for the same joint characteristics.

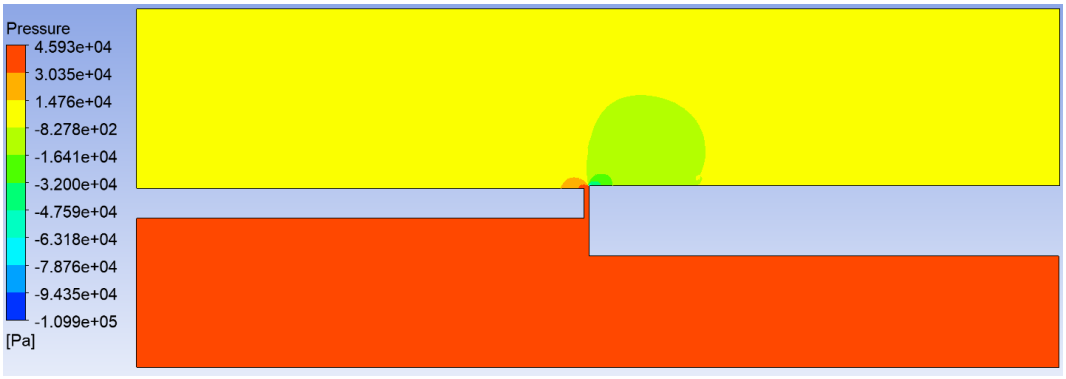

Figure 26- Pressure [Pa] distribution of the flow through the chamber for 50 ft/s for a slope of 30º

In figure 27, a detailed view of the pressure distribution near the joint is shown. Here it can be appreciated that just before the slab there is a pressure increase due to the water stagnation as it was expected. Also, regarding the low pressures, it can be seen in the figure that the lowest pressure of the chamber is obtained just after the joint, taking a value of -109900 Pa (relative pressure). This point is extremely dangerous due to the possible generation of cavitation which can lead to an irreversible damage in the structure.

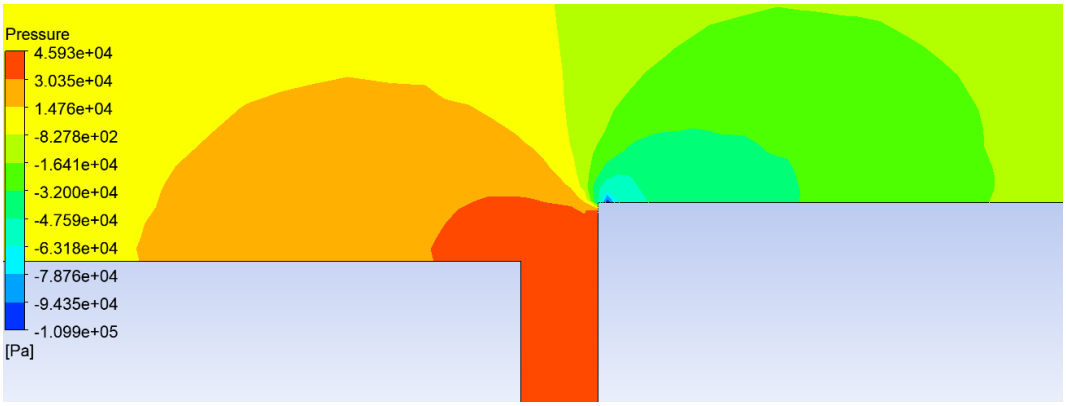

Figure 27 - Detailed pressure distribution near the joint for 50 ft/s for a slope of 30º

Figure 28 shows the horizontal static pressure distribution through the joint for the three velocities. It is seen that the values keep almost constant in the beginning but when the water reaches the second slab, there is a large pressure decrease. The pressure at this point must be carefully study as cavitation might occur.

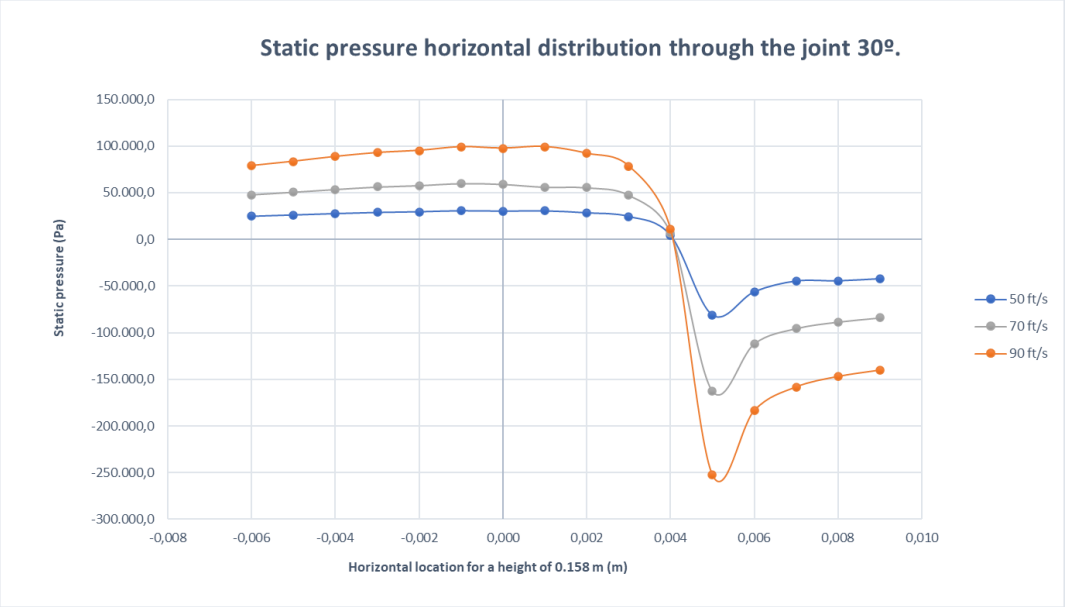

Figure 28- Static pressure horizontal distribution through the joint for 50, 70 and 90 ft/s velocities and 30º of slope

In figure 29 and 30 the velocity profile and phase distribution through the chamber are shown respectively. It can be clearly seen the free-surface and the border with the air in both cases. In figure 29, The turbulence generated just after the crack affect directly to the flow velocity close to the wall downstream the joint. Also, the free-surface keeps almost constant through the channel with a level of 0.26 mm.

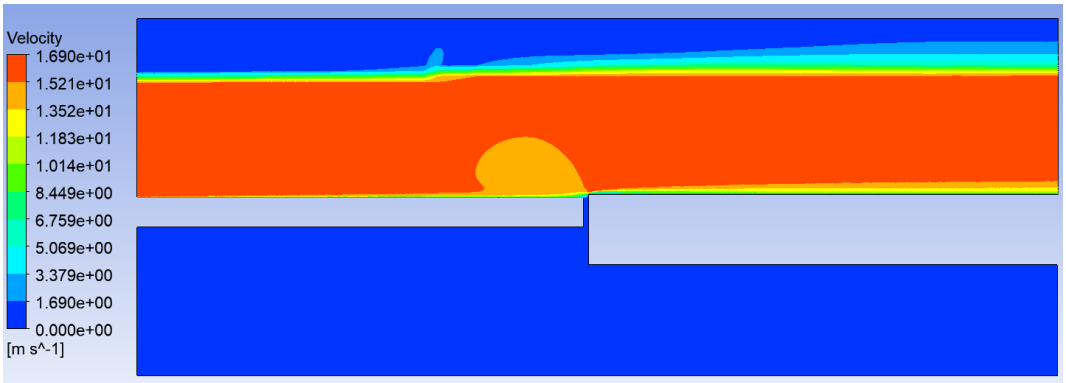

Figure 29- Velocity [m/s] profile of the flow through the chamber for 50 ft/s for a slope of 30º

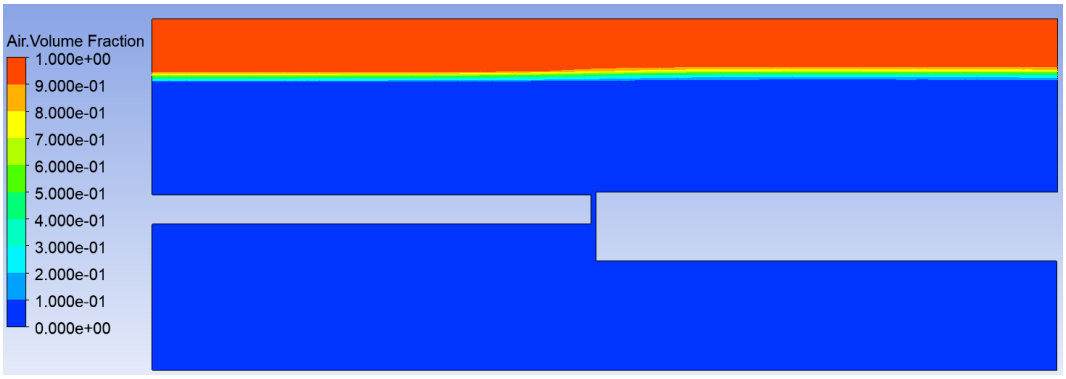

Figure 30-Phases distribution through the chamber for 50 ft/s for a slope of 30º

Finally, the velocity streamlines are shown in figure 30 where the stagnated water under the slabs is clearly appreciated.

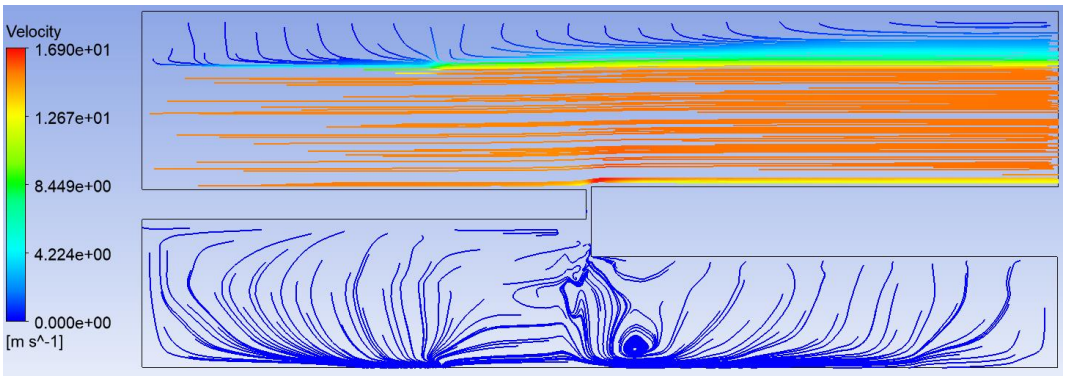

Figure 31 - Velocity streamlines through the chamber for 50 ft/s for a slope of 30º

4.2.2 Slope of 45º

In the next section, the water profile through the chamber is shown for a slope of 45º. Following the same pattern as in the section below, figure 32 shows the pressure distribution. It follows the same tendencies as with a lower slope where there is a pressure decrease just after the joint. The rest of the upper side of the chamber takes values of pressure near to the atmospheric pressure due to the free-surface.

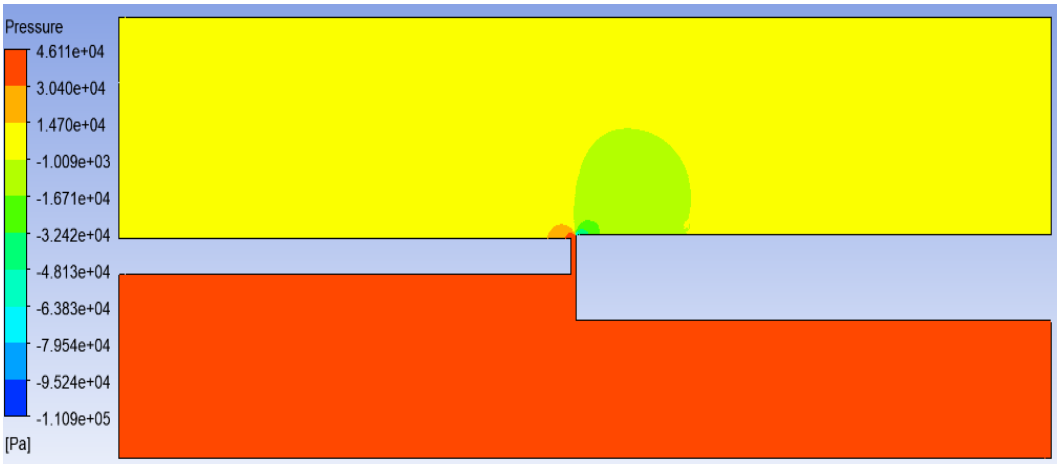

Figure 32- Pressure [Pa] distribution of the flow through the chamber for 50 ft/s for a slope of 45°

Figure 33 shows the pressure distribution near the joint for the case of a slope of 45° where it is easily seen the pressure increase before the joint and the pressure decrease just after it. The lowest pressure of the figure is located in the same point as in the section before, obtaining values that can be dangerous due to the possible generation of cavitation.

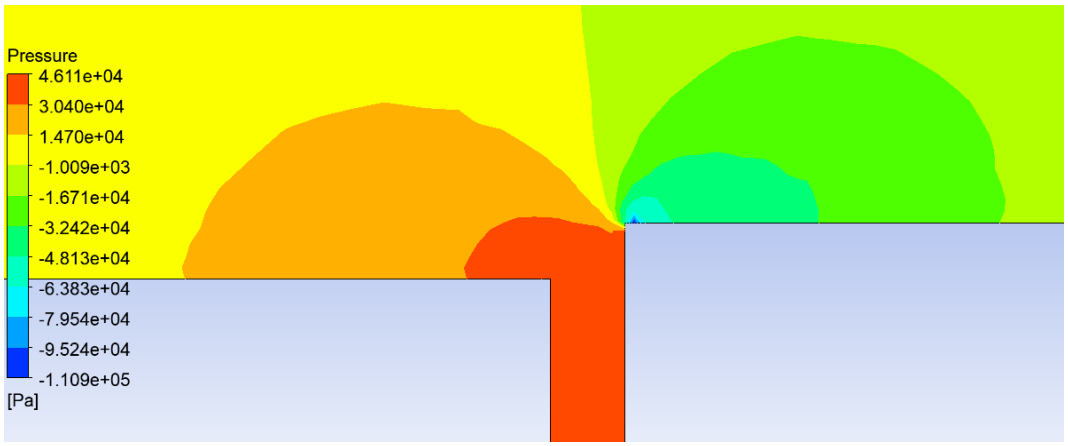

Figure 33-Detailed pressure distribution near the joint for 50 ft/s for a slope of 45°

Figure 34 shows the horizontal distribution of the static pressure through the joint in order to show more clearly the cavitation effect. The graphic shows a slight increase of the pressure due to the water stagnation in the beginning and when it reaches the second slab that is located in the 0.004 approximately, the pressure develops a great decrease just in 1 mm. Then, it rises again until almost the half of the pressure that had before. This reduction is more significant for larger velocities as it is shown so that it is more likely to generate cavitation in these cases.

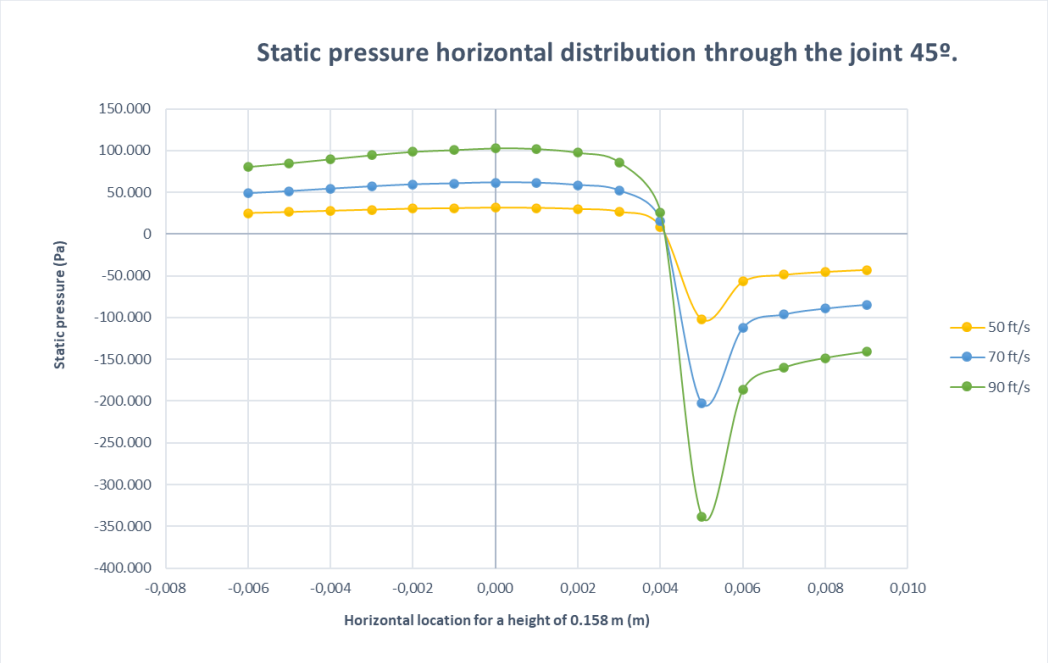

Figure 34-Static pressure horizontal distribution through the joint for 50, 70 and 90 ft/s velocities and 45° of slope

Figures 35, 36 and 37 show the velocity profile, the phases distribution and the velocity streamlines respectively. The water behavior follows the same patterns as in the previous section with lower slope. Figure 36 shows clearly the free-surface between the water and the air. Also, the water stagnation under the slabs is easily appreciated in figure 37.

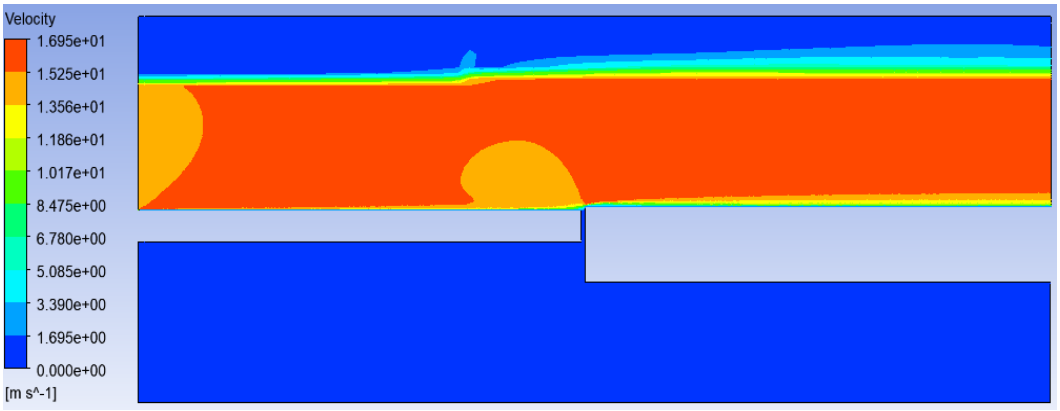

Figure 35- Velocity [m/s] profile of the flow through the chamber for 50 ft/s for a slope of 45°

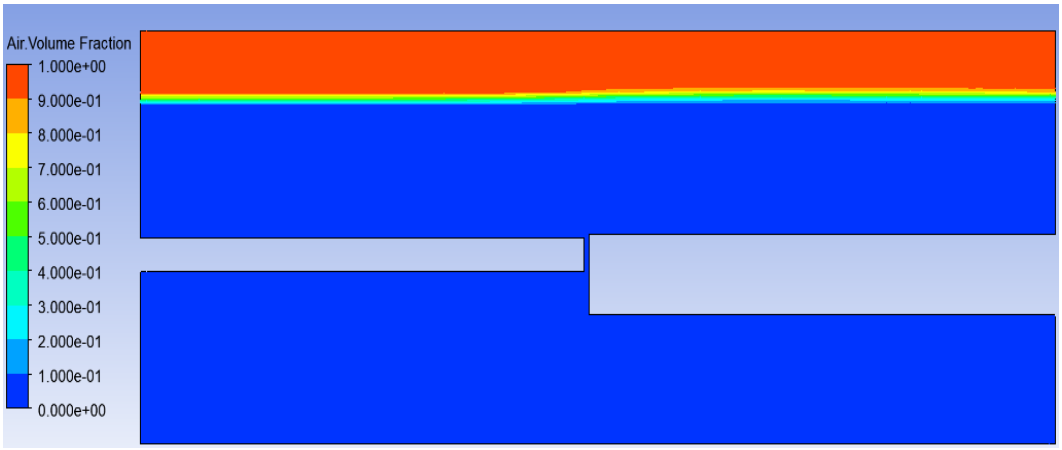

Figure 36 - Phases distribution through the chamber for 50 ft/s for a slope of 45°

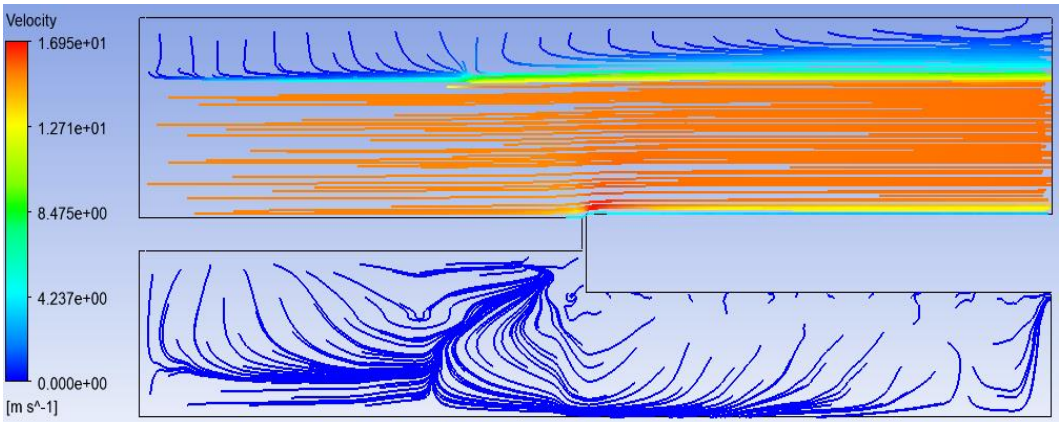

Figure 37-Velocity streamlines through the chamber for 50 ft/s for a slope of 45°

Figure 38 and 39 show the dynamic and static pressures distribution through the joint for 50 ft/s (21,34 m/s) of mean velocity of the flow. The mid-height of the offset is located 153 mm from the bottom of the chamber. The dynamic pressure has been calculated with equation 3 taking the value of the velocity of each point. Both graphics show a larger gradient in the first milimetres starting from the top, and then both the velocity and the static pressure remains almost constant for the lower values. From 149 mm to the bottom of the chamber has not been introduced as the tendency remains the same for the hole cavity and the values do not have significant changes.

Also, comparing both graphics can be easily observed the stagnation phenomena. While the water gets stagnated in the joint, the velocity decreases and with it the dynamic pressure decreases, increasing the static pressure until it achieves constant values when the velocity is nearly zero.

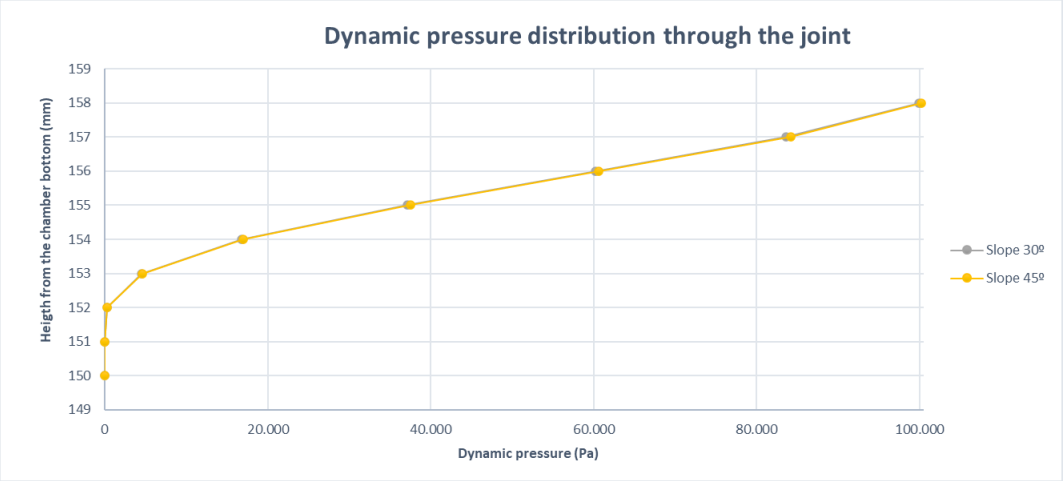

Figure 38-Dynamic pressure distribution through the joint for open channel tests with different slopes for 50 ft/s

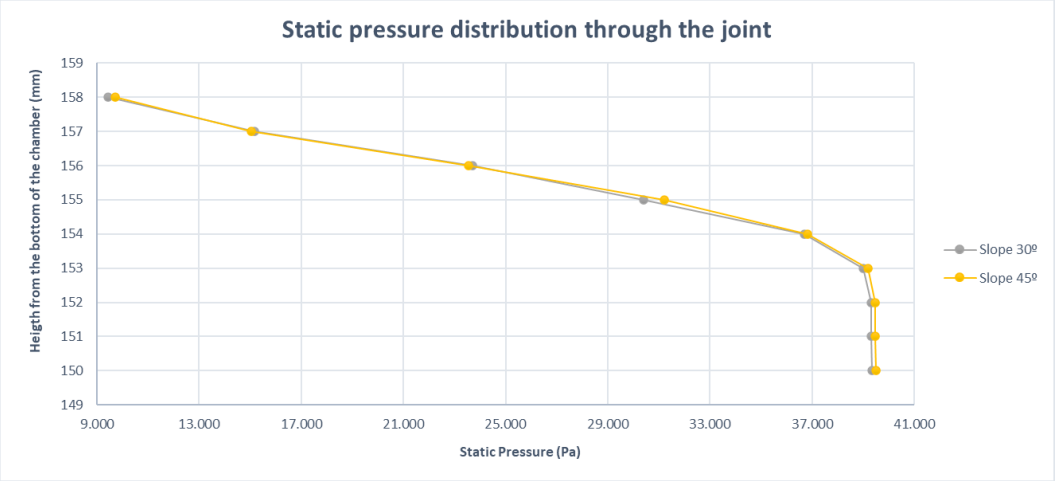

Figure 39- Static pressure distribution through the joint for open channel tests with different slopes for 50 ft/s

In the figures below it can be easily concluded that the pressure has the greatest gradient in the offset and then remains almost constant in all the cavity. However, the obtained values have a high similitude between both slopes. For higher velocities this pattern keeps the same obtaining similar results in both 30º and 45º slopes. It can be easily concluded from this fact that the gravity does not have much effect in the obtained pressures, and other factors such as the velocity of the flow or the gap and the offset of the joint are the main sources of the pressure difference in this kind of experiments.

5 Discussion

The results obtained in the close channel simulations follow the same patterns as it was expected from the experimental tests. An increase in the mean velocity of the channel result in a higher uplift pressure. Also, increasing the offset height of the joint, increases the uplift pressure generated. It can be due to the boundary layer velocity. The velocity mid-height the joint offset is larger for bigger offsets as it is farther to the wall. The stagnation pressure, as explained in the theory, is directly affected by this velocity so that higher offsets will generate larger uplifts pressures. From table 5 and 9 can be also concluded that the radius-edged geometries generate similar pressures to the sharp-edged geometry of a wider gap joint.

On the other hand, tables 10, 11 and 12 show a comparation between the numerical values obtained for each geometry. It is observed that that the variation of the uplift pressure value from the unvented to the discharged configuration keep almost constant, being a 3% the largest difference. These results were expected because the discharge values taken from the experimental reports were between 0.7-1.7 kg/s, so in general trends, the results of the vented geometries were a little lower.

Table 10 - Comparation between uplifting pressures in sealed and vented cavities for sharp-edged geometries

Velocity (ft/s)	Uplift Pressure (Pa)		
	Sealed	Vented	Variation (%)
50	43389.38	42127.94	3%
70	84853.78	83047.97	2%
90	141031.37	138691.41	2%

Table 11 - Comparation between uplifting pressures in sealed and vented cavities for chamber-edged geometries

Velocity (ft/s)	Uplift Pressure (Pa)		
	Sealed	Vented	Variation (%)
50	62253.42	62499.62	0,39%
70	122456.13	122856.88	0,32%
90	203983.91	204627.67	0,31%

Table 12 - Comparation between uplifting pressures in sealed and vented cavities for radius-edged ceometries

Velocity	Uplift Pressure (Pa)		
(ft/s)	Sealed	Vented	Variation (%)
50	46704.13	45469.22	3%
70	92172.55	90863.97	1%
90	154179.84	153152.21	1%

Those tables explain the increase in the error from the results of the vented cavities related to the sealed ones shown in the previous section. From the experimental data, the introduction of the discharge flow rate should decrease the pressure around a 7% for most of the cases, but this value keeps almost constant in the numerical analysis.

First of all, the discharge flow rate is taken from the graphics shown in the experimental report (Frizell, 2019). However, the report does not give data on the dimensions of the discharge crack, neither its exact location in the chamber, only the unit discharge flow rates are shown. This can be the source of different error that will lead to a lack of accuracy in the comparations.

Secondly, further investigations confirm that the discharge data provided in the report is not very reliable. For example, following the information given by the report, for a smaller gap, higher discharge values are obtained under the slab, which is not a sensible result. In the report it is justified that there is a back pressure under the joint as the discharge does not have the capacity to drain all the water flowing through the crack. Therefore, more precise analysis of the discharge flow under the spillway slabs is required for future research (Wahl, 2019).

Regarding the results obtained in the simulations of the chamber with different slopes, the next values of uplift pressure have been obtained. In order to calculate these values, the same criteria have been taken as in the water tunnel. The difference between the pressure under and above the slab has been calculated. The two points were chosen the same as in the close channel simulations. Table 13 shows the obtained values for each velocity.

Table 13 - Comparation between uplifting pressures in 30° and 45° slopes channels for sharp-edged geometry 1/8-inch offset 1/8-inch gap.

Velocity	Uplift Pressure (Pa)		
(ft/s)	30 degree	45 degree	Difference (%)
50	41470.1	41741.56	0,65%
70	80523.5	80801.1	0,34%
90	133858.9	134144.79	0,21%

As it is stated in the table, a little increase is observed in the uplift pressures with the increase of the slope angle. Anyway, there is not a large difference between both cases. This result was expected because the dominant forces of the pressures are not gravity forces but the offset geometries. That is why for a same joint configuration but different slopes, similar uplift pressures were expected.

On the other hand, analyzing the horizontal distribution of the statics pressures through the joint it has been seen that the slope of the channel has an effect in the cavitation. Figure 40 shows the static pressure distribution for a flow with a mean velocity of 50 ft/s for both slopes. It is seen that the flow has similar pressure before the joint, but when it reaches the crack, the pressure decreases to lower values in the case of 45º slope.

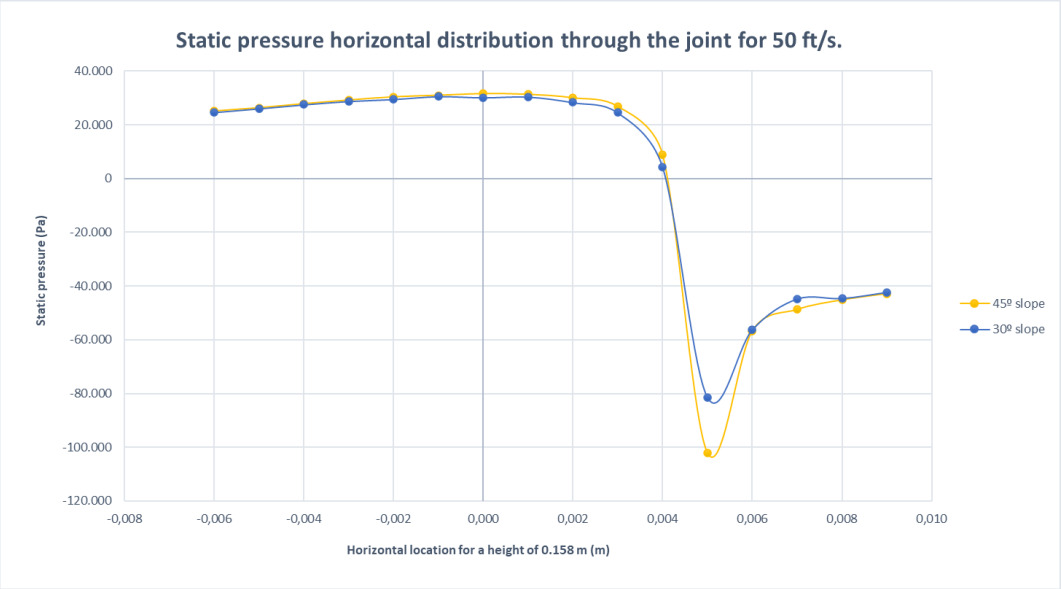

Figure 40-Static pressure horizontal distribution through the joint for 50 ft/s velocity

In the case of the 90 ft/s the graphic follows the same tendency but this time, the difference is even higher as it is seen in figure 41. This means that for bigger slopes, the cavitation has more effect than in smaller slopes.

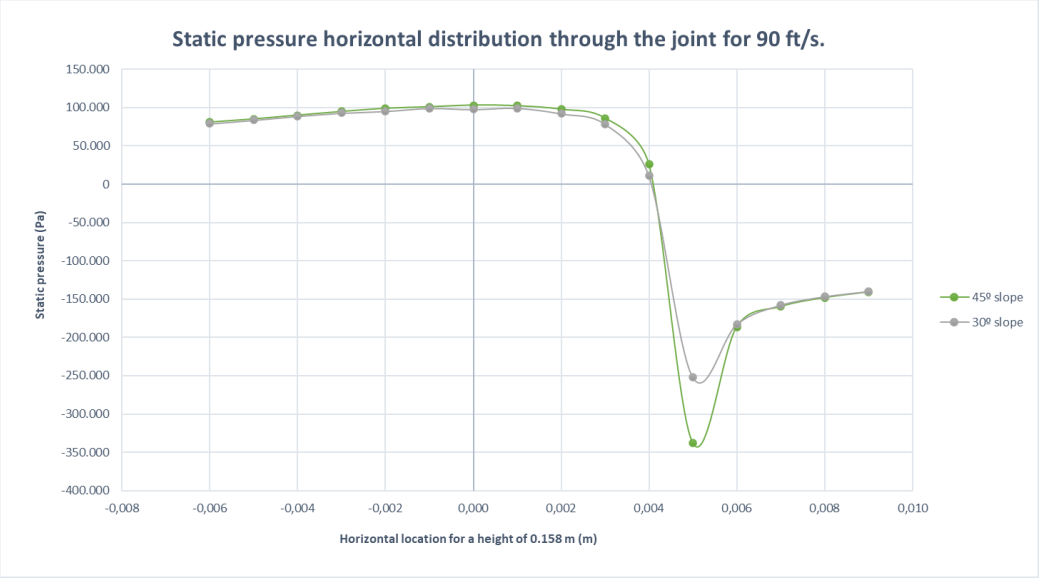

Figure 41- Static pressure horizontal distribution through the joint for 90 ft/s velocity

6 Conclusions

6.1 Study results

In conclusion, regarding the pressure effect on the slabs, hydraulic jacking is a significant problem that must be taken into consideration when building a spillway, especially when it is expected to be in use for many years. It is necessary to know the risk of an inappropriate spillway design which can lead to the flow of water through the joints that will generate high pressures. For this purpose, many researches have been made, and show that those pressures are definitely related to the joint gap width or the offset, as well as the mean flow velocity.

Regarding the results of the open channel simulations, the uplift pressures follow the same patterns and take similar values in both slopes. This verifies that the gravity is not the mean force in the experiment and other factors have more importance regarding the pressure in the joints such as the flow velocity. Also, an analysis on the pressure distribution just after the joint shows that the slope angle has a negative effect in the cavitation as it is more probable to face this problem with bigger slopes.

The aim of the project was to obtain a numerical model which could study the effect of the different joint geometries on the water behavior. The results show that the model represents with high accuracy the pressures generated under the slabs for sealed cavities but further analysis is required into the vented geometries as the report does not give precise information related to the discharge rate. Anyway, the results obtained for the vented cavity geometries do not exceed more than the 15% in the worst cases, which can also be acceptable.

6.2 Outlook

After analyzing the study and the experimental reports, further information is needed in order to obtain more accurate results. The Bureau of Reclamations plants to build a new laboratory model in order to analyze the pressures and flow rates through the joints but this time some variables that were not measured in the previous experiments will be measured such us the boundary layer velocity profiles, or the back pressure under the slabs.

Anyway, for future research in the field, it is suggested to do further investigation in the discharge rates of the cavities and the analysis on the uplift pressures under the slabs for these cases. Also, a new analysis in 3D could be interesting for future work as it is expected to give results closer to reality.

6.3 Perspectives

Hydropower is one of the main renewable sources in the world, and the first energy source in Sweden, but still exist certain disagreement if it should be considered green energy or not due to its possible consequences in the nature and the surrounding habitats. For this reason, many investigations are required in order to improve the security of the dams and avoid any kind of disasters. In this way, the study of the effect of the water flow over the spillway is an important case of study as it has been the source of many accidents over the years.

References

A. Bayon, J. P. Toro, F. A. Bombardelli, J. Matos, and P. A. López-Jiménez, "Influence of VOF technique, turbulence model and discretization scheme on the numerical simulation of the non-aerated, skimming flow in stepped spillways," *J. Hydro-Environment Res.*, vol. 19, pp. 137–149, Mar. 2018, doi: 10.1016/J.JHER.2017.10.002.

A. Parsaie and A. H. Haghiabi, "The hydraulic investigation of circular crested stepped spillway," *Flow Meas. Instrum.*, vol. 70, Dec. 2019, doi: 10.1016/J.FLOWMEASINST.2019.101624.

A. Vakil and S. I. Green, "Stagnation pressure, the Bernoulli equation, and the steady-flow energy equation," *Int. J. Mech. Eng. Educ.*, vol. 39, no. 2, pp. 130–138, 2011, doi: 10.7227/IJMEE.39.2.4.

B. Dargahi, "Experimental Study and 3D Numerical Simulations for a Free-Overflow Spillway," *J. Hydraul. Eng.*, vol. 132, no. 9, pp. 899–907, Sep. 2006, doi: 10.1061/(ASCE)0733-9429(2006)132:9(899)

B. M. Savage and M. C. Johnson, "Flow over Ogee Spillway: Physical and Numerical Model Case Study," *J. Hydraul. Eng.*, vol. 127, no. 8, pp. 640–649, Aug. 2001, doi: 10.1061/(ASCE)0733-9429(2001)127:8(640).

C. C. S. Song and F. Zhou, "Simulation of Free Surface Flow over Spillway," *J. Hydraul. Eng.*, vol. 125, no. 9, pp. 959–967, Sep. 1999, doi: 10.1061/(ASCE)0733-9429(1999)125:9(959).

D. G. Kim and J. H. Park, "Analysis of Flow Structure over Ogee-Spillway in Consideration of Scale and Roughness Effects by Using CFD Model," *KSCE J. Civ. Eng.*, vol. 9, no. 2, p. 161, 2005.

D. R. Shaymaa and A. M. Alhashimi, "CFD Modeling of Flow over Ogee Spillway by Using Different Turbulence Models," Accessed: May 13, 2022. [Online]. Available: www.semargroups.org,.

E. Fadaei-Kermani and G. A. Barani, "Numerical Simulation of Flow over Spillway Based on the CFD Method," *Sci. Iran.*, vol. 21, no. 1, pp. 91–97, 2014, [Online]. Available: http://scientiairanica.sharif.edu/article_1612.html.

G. W. Frey and D. M. Linke, "Hydropower as a renewable and sustainable energy resource meeting global energy challenges in a reasonable way," *Energy Policy*, vol. 30, no. 14, pp. 1261–1265, Nov. 2002, doi: 10.1016/S0301-4215(02)00086-1.

Hepler, T.E. & Johnson, P.L. 1988. "Analysis of spillway failures by uplift pressure," *J. Hydraul. Eng.*, Proceedings of the 1988 National Conference on Hydraulic Engineering and International Symposium on Model-Prototype Correlations, ASCE, Colorado Springs, Colorado, Aug. 8–12, 1988.

H. Zaïdi, S. Fohanno, R. Taïar, and G. Polidori, “Turbulence model choice for the calculation of drag forces when using the CFD method,” *J. Biomech.*, vol. 43, no. 3, pp. 405–411, Feb. 2010, doi: 10.1016/J.JBIOMECH.2009.10.010.

Johnson, P. L. "Research into Uplift on Steep Chute Lateral Linings," USBR, Denver, Colorado, 1976.

J. Wang, S. G. Weng, S. S. Wu, X. D. Hu, and X. Yang, “The visualization of flow field around circular cylinders by fluent standard k-ϵ turbulence model,” *IOP Conf. Ser. Earth Environ. Sci.*, vol. 344, no. 1, Nov. 2019, doi: 10.1088/1755-1315/344/1/012134.

J. Yang, P. Teng, and C. Lin, “Air-vent layouts and water-air flow behaviors of a wide spillway aerator,” *Theor. Appl. Mech. Lett.*, vol. 9, no. 2, pp. 130–143, Mar. 2019, doi: 10.1016/J.TAML.2019.02.009.

J. Zhong, M. Bollen, and S. Rönnberg, “Towards a 100% renewable energy electricity generation system in Sweden,” *Renew. Energy*, vol. 171, pp. 812–824, Jun. 2021, doi: 10.1016/J.RENENE.2021.02.153.

J. F. Melo, A. N. Pinheiro, and C. M. Ramos, “Forces on Plunge Pool Slabs: Influence of Joints Location and Width,” *J. Hydraul. Eng.*, vol. 132, no. 1, pp. 49–60, Jan. 2006, doi: 10.1061/(ASCE)0733-9429(2006)132:1(49).

K. W. Frizell, F. M. Renna, and J. Matos, “Cavitation Potential of Flow on Stepped Spillways,” *J. Hydraul. Eng.*, vol. 139, no. 6, pp. 630–636, Jun. 2013, doi: 10.1061/(ASCE)HY.1943-7900.0000715.

M. Tabbara, J. Chatila, and R. Awwad, “Computational simulation of flow over stepped spillways,” *Comput. Struct.*, vol. 83, no. 27, pp. 2215–2224, Oct. 2005, doi: 10.1016/J.COMPSTRUC.2005.04.005.

N. Fen, D. B. Kozlov, and I. S. Rumyantsev, “Hydraulic Studies of Stepped Spillways of Various Design,” *Power Technol. Eng.*, vol. 49, no. 5, pp. 337–344, Jan. 2016, doi: 10.1007/S10749-016-0625-7.

Ö. Kocaer and A. Yarar, “Experimental and Numerical Investigation of Flow Over Ogee Spillway,” *Water Resour. Manag.*, vol. 34, no. 13, pp. 3949–3965, Oct. 2020, doi: 10.1007/S11269-020-02558-9.

R. A. Karim and J. R. Mohammed, “A comparison study between CFD analysis and PIV technique for velocity distribution over the Standard Ogee crested spillways,” *Heliyon*, vol. 6, no. 10, Oct. 2020, doi: 10.1016/J.HELIYON.2020.E05165.

T. L. Wahl, “Effect of boundary layer conditions on uplift pressures at open offset spillway joints,” *Sustain. Safe Dams Around World*, pp. 2039–2048, Sep. 2019, doi: 10.1201/9780429319778-182.

T. Wahl, K. Frizell, and H. Falvey, “Uplift Pressures below Spillway Chute Slabs

at Unvented Open Offset Joints," *J. Hydraul. Eng.*, vol. 145, p. 4019039, Nov. 2019, doi: 10.1061/(ASCE)HY.1943-7900.0001637.

V. Fiorotto and P. Salandin, "Design of Anchored Slabs in Spillway Stilling Basins," *J. Hydraul. Eng.*, vol. 126, no. 7, pp. 502–512, Jul. 2000, doi: 10.1061/(ASCE)0733-9429(2000)126:7(502).

Z. Mu, Z. Zhang, and T. Zhao, "Numerical Simulation of 3-D Flow Field of Spillway based on VOF Method," *Procedia Eng.*, vol. 28, pp. 808–812, Jan. 2012, doi: 10.1016/J.PROENG.2012.01.814.